Supersymmetric constraints from $B_s \to \mu^+\mu^-$ and $B \to K^*\mu^+\mu^-$ observables

F. Mahmoudi,[a,1] **S. Neshatpour**[b] **and J. Orloff**[b]

[a] *CERN Theory Division, Physics Department,*
CH-1211 Geneva 23, Switzerland

[b] *Clermont Université, Université Blaise Pascal, CNRS/IN2P3,*
LPC, BP 10448, 63000 Clermont-Ferrand, France

E-mail: mahmoudi@in2p3.fr, neshatpour@clermont.in2p3.fr,
orloff@in2p3.fr

ABSTRACT: We study the implications of the recent LHCb limit and results on $B_s \to \mu^+\mu^-$ and $B \to K^*\mu^+\mu^-$ observables in the constrained SUSY scenarios. After discussing the Standard Model predictions and carefully estimating the theoretical errors, we show the constraining power of these observables in CMSSM and NUHM. The latest limit on $\mathrm{BR}(B_s \to \mu^+\mu^-)$, being very close to the SM prediction, constrains strongly the large $\tan\beta$ regime and we show that the various angular observables from $B \to K^*\mu^+\mu^-$ decay can provide complementary information in particular for intermediate $\tan\beta$ values.

---

[1]On leave from Clermont Université, Université Blaise Pascal, CNRS/IN2P3,
LPC, BP 10448, 63000 Clermont-Ferrand, France.

Contents

1 Introduction

The rare decays $B_s \to \mu^+\mu^-$ and $B \to K^*\mu^+\mu^-$ are sensitive probes of new particles arising in the extensions of the Standard Model (SM) and in particular Supersymmetry (SUSY). The measurements of these decays provide important constraints on the masses of new particles which are too heavy to be produced directly.

At large $\tan\beta$, the SUSY contributions to the decay $B_s \to \mu^+\mu^-$ is dominated by the exchange of neutral Higgs bosons, and it has been emphasised in many works [1–10] that this decay receives large enhancement, and very restrictive constraints can be obtained on the supersymmetric parameters. This decay is currently searched for by three LHC experiments: LHCb, CMS and ATLAS, and recently LHCb collaboration reported a very strong limit on the branching ratio of 4.5 $\times 10^{-9}$ [11] which is only about 15% larger than the SM prediction. This improved limit further constrains the SUSY parameter space. A possible signal, although with a low significance is also reported by the CDF collaboration [12].

The decay $B \to K^*\mu^+\mu^-$ on the other hand provides a variety of complementary observables as it gives access to angular distributions in addition to the differential branching fraction. Experimentally the exclusive $B \to K^*\mu^+\mu^-$ decay is easier to measure compared to the theoretically cleaner inclusive mode $B \to X_s\mu^+\mu^-$. However from a theoretical point

of view in the exclusive mode there are large uncertainties, which come mostly from the $B \to K$ form factors. Within the QCD factorisation [13, 14], simplifications can be made on the form factor description and by looking into the rich phenomenology of the various kinematic distributions, observables that have smaller dependency on the form factors can be defined [15, 16]. These observables prove to be important tools to study extensions of the SM [15–32] and they can provide valuable information on different sectors of the theory. The full determination of the angular distributions of $B \to K^* \mu^+ \mu^-$ constitutes a worthwhile challenge to the present and future experiments. Several angular observables have already been measured by Belle, Babar, CDF and LHCb. The most precise measurements come from the recent LHCb analyses with $1\,\mathrm{fb}^{-1}$ of integrated luminosity [33].

In this work we study for the first time the implications of the recent measurements of $B \to K^* \mu^+ \mu^-$ observables on constrained SUSY scenarios and update the constraints from $\mathrm{BR}(B_s \to \mu^+ \mu^-)$. Our numerical analysis is performed with SuperIso v3.3 [34, 35] and we study two constrained SUSY models: CMSSM and NUHM. To give some insight on the origin of these constraints, a mapping of the CMSSM parameter space into the Wilson coefficient subspace for the most relevant operators is also provided, which displays interesting partial correlations and hierarchies.

This paper is organised as follows: in section 2 we present a theoretical introduction to the decays $B_s \to \mu^+ \mu^-$ and $B \to K^* \mu^+ \mu^-$, provide the SM predictions and estimate the errors. In section 3 we summarise the experimental results and section 4 contains our numerical analysis of the constraints on the SUSY models that are obtained from the recent LHCb results. Conclusions are contained in section 5.

2   Observables, inputs and theoretical uncertainties

The effective Hamiltonian describing the $b \to s \ell^+ \ell^-$ transitions has the following generic structure[1][39, 40]:

$$\mathcal{H}_{\mathrm{eff}} = -\frac{4 G_F}{\sqrt{2}} V_{tb} V_{ts}^* \left[\sum_{i=1}^{6} C_i O_i + \sum_{i=7}^{10} \Big(C_i O_i + C_i' O_i' \Big) + \sum_{i=1}^{2} \Big(C_{Q_i} Q_i + C_{Q_i}' Q_i' \Big) \right] \quad (2.1)$$

where Q_1 and Q_2 are the scalar and pseudo-scalar operators and the primed operators are chirality flipped compared to the non-primed operators. Physics contributions at scales higher than μ are summarized in the so called Wilson coefficients $C_{i,Q_i}^{(\prime)}(\mu)$ (a typical choice for the scale is m_b for B decays). The Wilson coefficients include contributions from all particles heavier than $\mu_b = \mathcal{O}(m_b)$. In the SM these contributions are the top quark and the electroweak bosons and in BSM possible heavy NP particles are also summarised in the Wilson coefficients. The local operators $O_i^{(\prime)}$ and $Q_i^{(\prime)}$ include the long distance contributions from scales lower than μ_b. In the SM the primed and (pseudo-)scalar operators are either highly suppressed or absent. The most relevant operators for our work are

$$O_7 = \frac{e}{(4\pi)^2} m_b (\bar{s} \sigma^{\mu\nu} P_R b) F_{\mu\nu} , \qquad O_8 = \frac{g}{(4\pi)^2} m_b (\bar{s} \sigma^{\mu\nu} T^a P_R b) G_{\mu\nu}^a , \quad (2.2)$$

---

[1]We neglect the doubly Cabibbo-suppressed contributions of order $V_{ub} V_{us}^*$.

$$O_9 = \frac{e^2}{(4\pi)^2}(\bar{s}\gamma^\mu P_L b)(\bar{\ell}\gamma_\mu \ell) , \qquad O_{10} = \frac{e^2}{(4\pi)^2}(\bar{s}\gamma^\mu P_L b)(\bar{\ell}\gamma_\mu \gamma_5 \ell) ,$$

$$Q_1 = \frac{e^2}{(4\pi)^2}(\bar{s}P_R b)(\bar{\ell}\,\ell) , \qquad Q_2 = \frac{e^2}{(4\pi)^2}(\bar{s}P_R b)(\bar{\ell}\gamma_5 \ell) ,$$

where $P_{R,L} = (1 \pm \gamma_5)/2$ denote the chiral projectors and m_b is the $\overline{MS}$ mass of the b quark. A full list of the operators as well as the analytical expressions for all the Wilson coefficients can be found in [35]. The renormalisation group equations for C_1–C_8 are given in [41], for C_{Q_1} and C_{Q_2} in [1] and we calculated the running of C_9 which is given in appendix C.

2.1 $B_s \to \mu^+\mu^-$

Stringent 95% C.L. limit on the untagged branching ratio $BR_{\mathrm{untag}}(B_s \to \mu^+\mu^-) < 4.5 \times 10^{-9}$ has recently been obtained by the LHCb collaboration [11]. Taking into account the precise measurement [42] of the fractional decay width difference between the B_s heavy and light mass eigenstates, $y_s \equiv \Delta\Gamma_{B_s}/(2\Gamma_{B_s}) = 0.088 \pm 0.014$, this limit on the untagged branching ratio can be translated into an even stronger limit on the CP-averaged branching ratio $BR(B_s \to \mu^+\mu^-) \equiv \frac{1}{2}BR(B_s^0 \to \mu^+\mu^-) + \frac{1}{2}BR(\bar{B}_s^0 \to \mu^+\mu^-)$, reading [43–45]

$$BR(B_s \to \mu^+\mu^-) = (1 - y_s)BR_{\mathrm{untag}}(B_s \to \mu^+\mu^-) < 4.1 \times 10^{-9} \text{ at 95\% C.L.} \qquad (2.3)$$

where we assumed an SM-like scenario. In terms of Wilson coefficients, this average branching ratio is expressed as [35, 46]:

$$BR(B_s \to \mu^+\mu^-) = \frac{G_F^2 \alpha^2}{64\pi^3} f_{B_s}^2 m_{B_s}^3 |V_{tb}V_{ts}^*|^2 \tau_{B_s} \sqrt{1 - \frac{4m_\mu^2}{m_{B_s}^2}} \qquad (2.4)$$

$$\times \left\{ \left(1 - \frac{4m_\mu^2}{m_{B_s}^2}\right) |C_{Q_1} - C'_{Q_1}|^2 + \left|(C_{Q_2} - C'_{Q_2}) + 2(C_{10} - C'_{10})\frac{m_\mu}{m_{B_s}}\right|^2 \right\} .$$

In the Standard Model, only C_{10} is non-vanishing and gets its largest contributions from a Z penguin top loop (75%), and from a charmed box diagram (24%). With the inputs of table 2, $C_{10} = -4.21$, from which $BR(B_s \to \mu^+\mu^-)|_{SM} = (3.53 \pm 0.38) \times 10^{-9}$. The latest experimental limit thus severely restraints the room for new physics, and its proximity with the 2σ upper value calls for a discussion of the uncertainties in this SM prediction.

The main uncertainty comes from the B_s decay constant f_{B_s}, which has recently been re-evaluated by independent lattice QCD groups of table 1. Their 4.3% uncertainties agree, as do their results within these uncertainties, so that we have chosen an average of these three results in what follows. This implies a 8.7% uncertainty on the branching ratio.

Notice this range covers the recently published result $f_{B_s} = 225 \pm 4\,\mathrm{MeV}$ of McNeile et al. [51], whose lower value and striking precision dominates any weighted average including it, like the one in [52] ($227 \pm 4\,\mathrm{MeV}$) proposed by one of the authors of [51], or the one in [53]: $227 \pm 6\,\mathrm{MeV}$. The smallness of the extrapolation error in this work raises a number of new questions, and we prefer to keep our naive but more conservative average. This choice has however little effect on the new physics applications we have in mind, as these depend mostly on the lower end of that range.

Lattice QCD Group	ref.	f_{B_s}	f_B
ETMC-11	[47]	$232 \pm 10\,\mathrm{MeV}$	$195 \pm 12\,\mathrm{MeV}$
Fermilab-MILC-11	[48, 49]	$242 \pm 9.5\,\mathrm{MeV}$	$197 \pm 9\,\mathrm{MeV}$
HPQCD-12	[50]	$227 \pm 10\,\mathrm{MeV}$	$191 \pm 9\,\mathrm{MeV}$
Our choice		$234 \pm 10\,\mathrm{MeV}$	$194 \pm 10\,\mathrm{MeV}$

Table 1. Average of lattice QCD results used in this work.

Another potential source of uncertainty comes from the choice of scale at which the fine structure constant is used in eq. (2.4): there is a non-negligible 4% difference between the running $\overline{MS}$ couplings $\hat{\alpha}(m_b) = 1/133$ and $\hat{\alpha}(m_Z) = 1/128$. If the first choice may seem natural, the weak couplings involved in the top Z-penguin (or charmed box) are closer to the weak scale, and do not run below it, as discussed in ref. [54]. We thus take that last value, as well as $\sin^2 \hat{\theta}_W(m_Z) = 0.2312$ in the expression of eq. (2.4). This may seem at odds with the conclusion of ref. [54], that choosing $\hat{\alpha}(m_b)$ minimises the EW corrections to $B \to K^* \ell^+ \ell^-$. However, the EW corrections to $C_{7,9}$, which dominate the low q_{ll}^2 region of this last process, are opposite to the EW corrections for C_{10}, which controls $B_s \to \mu^+ \mu^-$. Having made this choice for the EM-coupling, we expect EW corrections to mostly absorb the remaining scale dependence in $\hat{\alpha}_{EM}(\mu)$, leaving a small, 2% uncertainty in the branching ratio.

The remaining theoretical uncertainties are smaller thanks to the NNLO treatment of QCD corrections: increasing the low scale μ_b (or the matching scale μ_W) by a factor of 2 induces a 1.4% (or respectively 2%) effect.

Finally, parametric uncertainties from the top mass (1.3%), from the B_s lifetime (1.8%) and from the CKM element V_{ts} (5%), will reduce in the future. Adding all these (small) errors in quadrature, we thus get a Standard Model prediction assorted with an 11% uncertainty:

$$BR(B_s \to \mu^+ \mu^-) = (3.53 \pm 0.38) \times 10^{-9} \ . \tag{2.5}$$

This value is compatible with recent SM predictions for this observable, *e.g.* by the CKMfitter group [55], for which the uncertainties are reduced by the use of other flavour information.

2.2 $B \to K^* \mu^+ \mu^-$

Considering the $\bar{K}^*$ meson to be on-shell, the differential decay distribution of the $\bar{B}^0 \to \bar{K}^*(\to K^- \pi^+)\ell^+ \ell^-$ decay can be written in terms of three angles θ_ℓ, θ_{K^*}, ϕ and the invariant dilepton mass squared (q^2) [15, 22]:

$$d^4\Gamma = \frac{9}{32\pi} J(q^2, \theta_\ell, \theta_{K^*}, \phi)\, dq^2\, d\cos\theta_\ell\, d\cos\theta_{K^*}\, d\phi \ . \tag{2.6}$$

In the above equation θ_ℓ is the angle between ℓ^- and $\bar{B}^0$ in the rest frame of the dilepton, θ_{K^*} is the angle between K^- and $\bar{B}^0$ in the $\bar{K}^*$ rest frame and ϕ is the angle

$m_B = 5.27950\,\text{GeV}$	[56]	$m_{B_s} = 5.3663\,\text{GeV}$	[56]
$m_{K^*} = 0.89594\,\text{GeV}$	[56]	$|V_{tb}V_{ts}^*| = 0.0403^{+0.0011}_{-0.0007}$	[56]
$m_b^{\overline{MS}}(m_b) = 4.19^{+0.18}_{-0.06}\,\text{GeV}$	[56]	$m_c^{\overline{MS}}(m_c) = 1.29^{+0.05}_{-0.11}\,\text{GeV}$	[56]
$m_t^{pole} = 172.9 \pm 0.6 \pm 0.9\,\text{GeV}$	[56]	$m_\mu = 0.105658\,\text{GeV}$	[56]
$\alpha_s(M_Z) = 0.1184 \pm 0.0007$	[56]	$\hat{\alpha}_{em}(M_Z) = 1/127.916$	[56]
$\alpha_s(\mu_b) = 0.2161$		$\hat{\alpha}_{em}(m_b) = 1/133$	
$\sin^2 \hat{\theta}_W(M_Z) = 0.23116(13)$	[56]	$G_F/(\hbar c)^3 = 1.16637(1)\,\text{GeV}^{-2}$	[56]
$f_B = 194 \pm 10\,\text{MeV}$	Table 1	$\tau_B = 1.519 \pm 0.007\,\text{ps}$	[56]
$f_{B_s} = 234 \pm 10\,\text{MeV}$	Table 1	$\tau_{B_s} = 1.472 \pm 0.026\,\text{ps}$	[56]
$f_{K^*,\perp}(1\,\text{GeV}) = 0.185 \pm 0.009\,\text{GeV}$	[57]	$f_{K^*,\parallel} = 0.220 \pm 0.005\,\text{GeV}$	[57]
$a_{1,\perp}(1\,\text{GeV}) = 0.10 \pm 0.07$	[58]	$a_{1,\parallel}(1\,\text{GeV}) = 0.10 \pm 0.07$	[58]
$a_{2,\perp}(1\,\text{GeV}) = 0.13 \pm 0.08$	[58]	$a_{2,\parallel}(1\,\text{GeV}) = 0.09 \pm 0.05$	[58]
$\lambda_{B,+}(1\,\text{GeV}) = 0.46 \pm 0.11\,\text{GeV}$	[59]		
$\mu_b = m_b^{pole}$		$\mu_0 = 2M_W$	
$\mu_f = \sqrt{0.5 \times \mu_b}\,\text{GeV}$	[14]		

Table 2. Input parameters used in this work.

between the normals of the $\ell^+\ell^-$ plane and the $K^-\pi^+$ in the $\bar{B}^0$ rest frame. The angular dependence of $J(q^2, \theta_\ell, \theta_{K^*}, \phi)$ can be written as

$$
\begin{aligned}
J(q^2, \theta_\ell, \theta_{K^*}, \phi) =\ & J_1^s \sin^2 \theta_{K^*} + J_1^c \cos^2 \theta_{K^*} + (J_2^s \sin^2 \theta_{K^*} + J_2^c \cos^2 \theta_{K^*}) \cos 2\theta_\ell \\
& + J_3 \sin^2 \theta_{K^*} \sin^2 \theta_\ell \cos 2\phi + J_4 \sin 2\theta_{K^*} \sin 2\theta_\ell \cos \phi \\
& + J_5 \sin 2\theta_{K^*} \sin \theta_\ell \cos \phi + (J_6^s \sin^2 \theta_{K^*} + J_6^c \cos^2 \theta_{K^*}) \cos \theta_\ell \\
& + J_7 \sin 2\theta_{K^*} \sin \theta_\ell \sin \phi + J_8 \sin 2\theta_{K^*} \sin 2\theta_\ell \sin \phi \\
& + J_9 \sin^2 \theta_{K^*} \sin^2 \theta_\ell \sin 2\phi \ .
\end{aligned}
\tag{2.7}
$$

The angular coefficients J_i (see appendix A), are functions of q^2 and can be described in terms of eight transversity amplitudes $A_\perp^{L,R}$, $A_\parallel^{L,R}$, $A_0^{L,R}$, A_t, A_S. The transversity amplitudes up to corrections of $\mathcal{O}(\alpha_s)$ can be expressed in terms of seven independent form factors, $A_{0,1,2}, T_{1,2,3}$ and V. Since these form factors are hadronic quantities they require non-perturbative calculations and hence are the main source of uncertainty in the exclusive mode. But even if the form factors were known precisely the $\bar{B}^0 \to \bar{K}^* \ell^+ \ell^-$ decay would still need corrections emerging from non-factorisable effects which are related to the current-current operators O_1 and O_2, the QCD penguin operators O_3-O_6 and the chromomagnetic operator O_8. The non-factorisable corrections contribute to the decay amplitude by producing a virtual photon which decays into a lepton pair. When the $\bar{K}^*$

has a large energy (q^2 is small) and the decaying hadron ($\bar{B}^0$) is heavy, the non-factorisable corrections can be computed in the QCD factorisation framework [13, 14]. In the QCDf framework in the large recoil limit the seven independent form factors can be expanded in ratios of $1/m_b$ and $1/E_{K^*}$ [60, 61]. While α_s corrections to the form factors in QCDf have been calculated [61], the $1/m_b$ corrections are unknown. Neglecting $1/m_b$ corrections, the transversity amplitudes at NLO in α_s in the large recoil limit are[2] [15, 22, 23]:

$$A_\perp^{L,R} = N\sqrt{2}\sqrt{\lambda} \left[\left[(C_9 + C_9') \mp (C_{10} + C_{10}') \right] \frac{V(q^2)}{M_B + m_{K^*}} + \frac{2m_b}{q^2}\mathcal{T}_\perp^+ \right], \tag{2.8a}$$

$$A_\parallel^{L,R} = -N\sqrt{2}(M_B^2 - m_{K^*}^2) \left[\left[(C_9 - C_9') \mp (C_{10} - C_{10}') \right] \frac{A_1(q^2)}{M_B - m_{K^*}} + \frac{4m_b}{M_B}\frac{E_{K^*}}{q^2}\mathcal{T}_\perp^- \right], \tag{2.8b}$$

$$
\begin{aligned}
A_0^{L,R} = -\frac{N}{2m_{K^*}\sqrt{q^2}} &\Bigg\{ \left[(C_9 - C_9') \mp (C_{10} - C_{10}') \right] \\
&\times \left[(M_B^2 - m_{K^*}^2 - q^2)(M_B + m_{K^*})A_1(q^2) - \lambda\frac{A_2(q^2)}{M_B + m_{K^*}} \right] \\
&+ 2m_b \left[\frac{2E_{K^*}}{M_B}(M_B^2 + 3m_{K^*}^2 - q^2)\mathcal{T}_\perp^- - \frac{\lambda}{M_B^2 - m_{K^*}^2}\left(\mathcal{T}_\perp^- + \mathcal{T}_\parallel^- \right) \right] \Bigg\} \quad (2.8c)
\end{aligned}
$$

$$A_t = \frac{N}{\sqrt{q^2}}\sqrt{\lambda} \left[2(C_{10} - C_{10}') + \frac{q^2}{m_\ell m_b}(C_{Q_2} - C_{Q_2}') \right] \frac{E_{K^*}}{m_{K^*}}\xi_\parallel(q^2), \tag{2.8d}$$

$$A_S = -\frac{2N}{m_b}\sqrt{\lambda}(C_{Q_1} - C_{Q_1}')\frac{E_{K^*}}{m_{K^*}}\xi_\parallel(q^2), \tag{2.8e}$$

where E_{K^*} is the energy of the final vector meson in the B rest frame

$$E_{K^*} = \frac{M_B^2 + m_{K^*}^2 - q^2}{2M_B}, \tag{2.9}$$

and

$$N = \left[\frac{G_F^2 \alpha_{em}^2}{3 \cdot 2^{10}\pi^5 M_B^3}|V_{tb}V_{ts}^*|^2 q^2\sqrt{\lambda}\,\beta_\ell \right]^{1/2}, \qquad \beta_\ell = \sqrt{1 - \frac{4m_\ell^2}{q^2}}, \tag{2.10}$$

and λ is the triangle function $\lambda(M_B^2, m_{K^*}^2, q^2)$

$$\lambda = M_B^4 + m_{K^*}^4 + q^4 - 2(M_B^2 m_{K^*}^2 + m_{K^*}^2 q^2 + M_B^2 q^2). \tag{2.11}$$

Further explanation on what we use for $\mathcal{T}_{\perp,\parallel}^\pm$, $\xi_{\perp,\parallel}$, $A_{1,2}$ and V is given in appendix B.

For the differential distribution of the CP conjugate decay $B^0 \to K^*(\to K^+\pi^-)\ell^+\ell^-$, if we keep the definition of θ_ℓ to remain the same and replace K^- with K^+ for the definition of θ_{K^*} and consider ϕ to be the angle between the normals of the $\ell^+\ell^-$ plane and the $K^+\pi^-$ in the B^0 rest frame, we can use eq. (2.6) where J is replaced with $\bar{J}$. The function $\bar{J}(q^2, \theta_\ell, \theta_{K^*}, \phi)$ is obtained from eq. (2.7) by the replacements [62]

$$J_{1,2}^{(c,s)} \to \bar{J}_{1,2}^{(c,s)}, \qquad\qquad J_6^{(c,s)} \to -\bar{J}_6^{(c,s)}, \tag{2.12}$$

$$J_{3,4,7} \to \bar{J}_{3,4,7}, \qquad\qquad J_{5,8,9} \to -\bar{J}_{5,8,9}, \tag{2.13}$$

---

[2]For A_t and A_S, the α_s correction which emerges from describing A_0 in terms of $\xi_\parallel$ is very small and has been neglected.

where $\bar{J}$ is equal to J with all the weak phases conjugated. The change of sign for $J_{5,6,8,9}$ can be understood by considering that the CP conjugate decay leads to the transformations $\theta_\ell \to \pi - \theta_\ell$ and $\phi \to -\phi$ in eq. (2.7).

2.2.1 Observables

Integrating eq. (2.6) over all angles, the dilepton mass distribution can be written in terms of the angular coefficients [22, 23]:

$$\frac{d\Gamma}{dq^2} = \frac{3}{4}\left(J_1 - \frac{J_2}{3}\right) . \tag{2.14}$$

For the normalised forward-backward asymmetry A_{FB} we use [22, 23]:

$$A_{\text{FB}}(q^2) \equiv \left[\int_{-1}^{0} - \int_{0}^{1}\right] d\cos\theta_\ell \, \frac{d^2\Gamma}{dq^2 \, d\cos\theta_\ell} \bigg/ \frac{d\Gamma}{dq^2} = -\frac{3}{8}J_6 \bigg/ \frac{d\Gamma}{dq^2} , \tag{2.15}$$

where $J_i \equiv 2J_i^s + J_i^c$ for $i = 1, 2, 6$. The longitudinal polarisation fraction F_L can be constructed as the ratios of the transversity amplitudes and therefore contains less theoretical uncertainty from the form factors. For the longitudinal polarisation, F_L we have [15, 22]:

$$F_L(s) = \frac{-J_2^c}{d\Gamma/dq^2} . \tag{2.16}$$

An interesting observable is the zero-crossing of the forward-backward asymmetry (q_0^2). Neglecting the lepton masses and not considering the chirality flipped and scalar operators for the zero of A_{FB} we obtain

$$q_0^2 = \frac{-m_b}{C_9}\text{Re}\left[(M_B - m_{K^*})\frac{2E_{K^*}}{M_B}\frac{\mathcal{T}_\perp}{A_1} + (M_B + m_{K^*})\frac{\mathcal{T}_\perp^*}{V}\right] . \tag{2.17}$$

To calculate the zero of A_{FB} in our numerical analysis we have directly used the relation for A_{FB} (eq. (2.15)).

Another observable which is rather independent of hadronic input parameters is the isospin asymmetry which arises from non-factorizable effects. The non-factorizable effects depend on the charge of the spectator quark, and hence depending on whether the decaying B meson is charged or neutral, there will be a difference in the contribution of these effects to the decay width which can cause an isospin asymmetry. The (CP averaged) isospin asymmetry is defined as [20]

$$\frac{dA_I}{dq^2} = \frac{d\Gamma[B^0 \to K^{*0}\ell^+\ell^-]/dq^2 - d\Gamma[B^\pm \to K^{*\pm}\ell^+\ell^-]/dq^2}{d\Gamma[B^0 \to K^{*0}\ell^+\ell^-]/dq^2 + d\Gamma[B^\pm \to K^{*\pm}\ell^+\ell^-]/dq^2} . \tag{2.18}$$

In the SM, dA_I/dq^2 is at the percent level [14, 20], the smallness of the isospin asymmetry makes it sensitive to isospin-violating NP effects.

Other observables of interest are the transverse amplitudes which have a small dependence on the form factors and a large sensitivity to right-handed currents via C_7'. They are defined as [15, 16, 22, 63]

$$A_T^{(2)}(s) = \frac{J_3}{2 J_2^s} , \tag{2.19}$$

$$A_T^{(3)}(s) = \left(\frac{4(J_4)^2 + \beta_\ell^2 (J_7)^2}{-2J_2^c (2J_2^s + J_3)} \right)^{1/2} , \tag{2.20}$$

$$A_T^{(4)}(s) = \left(\frac{\beta_\ell^2 (J_5)^2 + 4(J_8)^2}{4(J_4)^2 + \beta_\ell^2 (J_7)^2} \right)^{1/2} , \tag{2.21}$$

as well as

$$A_{Im}(s) = \frac{J_9}{d\Gamma/dq^2} , \tag{2.22}$$

which is sensitive to the complex phases, but very small ($\mathcal{O}(10^{-3})$) in the SM.

All the observables can also be expressed in terms of the CP averaged angular coefficients S_i [22]. In particular, S_3, which has recently been measured by LHCb, can be related to F_L and $A_T^{(2)}$ by

$$S_3 = \frac{1}{2}(1 - F_L)A_T^{(2)} , \tag{2.23}$$

in the limit of vanishing lepton masses.

For the high q^2 region we follow [26], where the heavy quark effective theory (HQET) of [64] is used. In that framework improved Isgur-Wise form factor relations are used to extrapolate the lacking high q^2 form factors from the calculations of the low q^2 form factors and an operator product expansion in powers of $1/Q^2$, ($Q = (m_b, \sqrt{q^2})$), is used for the estimation of the long-distance effects from quark loops. For the low recoil region (high q^2), the following observables are proposed by [26]

$$H_T^{(1)} = \frac{\sqrt{2}J_4}{\sqrt{-J_2^c (2J_2^s - J_3)}} , \tag{2.24}$$

$$H_T^{(2)} = \frac{\beta_l J_5}{\sqrt{-2J_2^c (2J_2^s + J_3)}} , \tag{2.25}$$

$$H_T^{(3)} = \frac{\beta_l J_6^s}{2\sqrt{(2J_2^s)^2 - (J_3)^2}} . \tag{2.26}$$

These transversity observables have small hadronic uncertainties at high q^2.

2.2.2 Standard Model values and theoretical uncertainties

For our numerical analysis we have used the NLO relations for the transversity amplitudes in the ($1 < q^2 < 6 \, \text{GeV}^2$) region where we are sufficiently below the charm resonance threshold ($q^2 = m_c^2$) and far enough from the kinematic minimum where the decay amplitude is dominated by the photon pole. The input parameters can be found in table 2 and the SM Wilson coefficients are given in table 3. The available experimental values are given for q^2 bins which can be shown as $\langle \text{observable} \rangle_{[q_{\min}^2, q_{\max}^2]}$, in other words the dq^2 integration is over the $[q_{\min}^2, q_{\max}^2]$ bin. For normalised quantities like A_{FB} and F_L the numerator and denominator are integrated separately [15, 26]:

$$\langle A_{FB} \rangle_{[q_{\min}^2, q_{\max}^2]} = -\frac{3}{8} \frac{\langle J_6 \rangle_{[q_{\min}^2, q_{\max}^2]}}{\langle d\Gamma/dq^2 \rangle_{[q_{\min}^2, q_{\max}^2]}}, \tag{2.27}$$

$$\langle F_L \rangle_{[q_{\min}^2, q_{\max}^2]} = \frac{\langle -J_2^c \rangle_{[q_{\min}^2, q_{\max}^2]}}{\langle d\Gamma/dq^2 \rangle_{[q_{\min}^2, q_{\max}^2]}}. \tag{2.28}$$

$C_1(\mu_b)$	$C_2(\mu_b)$	$C_3(\mu_b)$	$C_4(\mu_b)$	$C_5(\mu_b)$	$C_6(\mu_b)$	$C_7^{\text{eff}}(\mu_b)$	$C_8^{\text{eff}}(\mu_b)$	$C_9(\mu_b)$	$C_{10}(\mu_b)$
-0.2610	1.0076	-0.0052	-0.0795	0.0004	0.0009	-0.2974	-0.1614	4.2297	-4.2068

Table 3. SM Wilson coefficients at $\mu_b = m_b^{\text{pole}}$ and $\mu_0 = 2M_W$ to NNLO accuracy in α_s.

Observable	SM prediction	(FF)	(SL)	(QM)	(CKM)	(Scale)
$10^7 \times BR(B \to K^*\mu^+\mu^-)_{[1,6]}$	2.32	± 1.34	± 0.04	$^{+0.04}_{-0.03}$	$^{+0.08}_{-0.13}$	$^{+0.09}_{-0.05}$
$\langle A_{FB}(B \to K^*\mu^+\mu^-)\rangle_{[1,6]}$	-0.06	± 0.04	± 0.02	± 0.01	—	—
$\langle F_L(B \to K^*\mu^+\mu^-)\rangle_{[1,6]}$	0.71	± 0.13	± 0.01	± 0.01	—	—
$q_0^2(B \to K^*\mu^+\mu^-)/\text{GeV}^2$	4.26	± 0.30	± 0.15	$^{+0.14}_{-0.04}$	—	$^{+0.02}_{-0.04}$

Table 4. SM predictions and errors.

We estimate the theoretical uncertainties for the SM values in the low q^2 region using two methods: one follows the approach of [65], and the second is based on a Monte Carlo method. Both methods give similar results. We consider five different sources of uncertainty. The errors from the form factors (FF) have been calculated by adding in quadrature the uncertainties due to V, A_1 and A_2 (11%, 13% and 14%, respectively [58]). For the unknown $1/m_b$ sub-leading corrections (SL), we have assumed 7% corrections to the $\mathcal{T}_{\perp,\parallel}$ terms in the transversity amplitudes[3], these corrections have been added in quadrature. Another group of errors is from the quark mass uncertainties (QM) which we have estimated by separately varying m_t^{pole}, $m_b^{\overline{MS}}$ and $m_c^{\overline{MS}}$ according to table 2 and added in quadrature. Another source of error comes from the uncertainty in the CKM matrix element combination $|V_{tb}V_{ts}^*|$ (CKM) which has been computed by considering the uncertainty given in table 2. The last source of error that we consider is the scale dependence (Scale) which we estimate by varying μ_b between $\mu_b/2$ and $2\mu_b$ (with $\mu_b = m_b^{pole}$). These five groups of errors for BR, A_{FB}, F_L and q_0^2 in the SM have been gathered in table 4. For the Standard Model predictions the primed coefficients (C'_{i,Q_1,Q_2}) as well as the scalar coefficients ($C_{Q_{1,2}}$) have been put to zero.

For the high q^2 region we have used the relative errors of table 2 in [26].

3 Experimental results

At present, the best upper limit for $\text{BR}(B_s \to \mu^+\mu^-)$ measured in a single experiment comes from LHCb [11]:

$$\text{BR}(B_s \to \mu^+\mu^-) < 4.5 \times 10^{-9} \tag{3.1}$$

at 95% C.L. This upper limit is followed by the result from CMS [66]:

$$\text{BR}(B_s \to \mu^+\mu^-) < 7.7 \times 10^{-9} \,. \tag{3.2}$$

---

[3]If for the (SL) error a 10% correction to the $\mathcal{T}_{\perp,\parallel}$ is considered the overall uncertainties will not have a significant change since they are dominated by the (FF) uncertainties.

Observable	SM prediction	Experiment
$10^7 \text{GeV}^2 \times \langle dBR/dq^2 \, (B \to K^* \mu^+ \mu^-) \rangle_{[1,6]}$	0.47 ± 0.27	$0.42 \pm 0.04 \pm 0.04$
$\langle A_{FB}(B \to K^* \mu^+ \mu^-) \rangle_{[1,6]}$	-0.06 ± 0.05	$-0.18^{+0.06+0.01}_{-0.06-0.01}$
$\langle F_L(B \to K^* \mu^+ \mu^-) \rangle_{[1,6]}$	0.71 ± 0.13	$0.66^{+0.06+0.04}_{-0.06-0.03}$
$q_0^2(B \to K^* \mu^+ \mu^-)/\text{GeV}^2$	$4.26^{+0.36}_{-0.34}$	$4.9^{+1.1}_{-1.3}$

Table 5. Experimental values and SM predictions (the theoretical errors are from adding in quadrature the different errors in table 4).

The CDF collaboration obtains a 95% C.L. upper limit [12]:

$$\text{BR}(B_s \to \mu^+ \mu^-) < 3.4 \times 10^{-8} \, , \tag{3.3}$$

together with a one sigma interval

$$\text{BR}(B_s \to \mu^+ \mu^-) = (1.3^{+0.9}_{-0.7}) \times 10^{-8} \, , \tag{3.4}$$

coming from an observed excess over the expected background.

For our numerical evaluations, we consider the LHCb limit, and accounting for 11% theoretical uncertainty (as explained in section 2.1), we impose the following limit at 95% C.L.[4]

$$\text{BR}(B_s \to \mu^+ \mu^-) < 5.0 \times 10^{-9} \, . \tag{3.5}$$

For $B \to K^* \mu^+ \mu^-$ related observables we also use the latest LHCb results which correspond to an integrated luminosity of $1\,\text{fb}^{-1}$ [33]. The results are summarised in table 5 where the experimental uncertainties are statistical and systematic. For comparison, the SM predictions with the corresponding theoretical errors (from the five sources of errors mentioned in table 4, added in quadrature) are also provided.

In addition to the observables in table 5, three other observables have also been measured using $1\,\text{fb}^{-1}$ of LHCb data namely S_3 and A_{Im} [33] and also very recently the isospin asymmetry A_I [67]. The reported results are:

$$\langle 2\, S_3(B \to K^* \mu^+ \mu^-) \rangle_{[1,6]} = 0.10^{+0.15+0.02}_{-0.16-0.01} \, , \tag{3.6}$$

$$\langle A_{Im}(B \to K^* \mu^+ \mu^-) \rangle_{[1,6]} = 0.07^{+0.07+0.02}_{-0.7-0.01} \, , \tag{3.7}$$

$$\langle A_I(B \to K^* \mu^+ \mu^-) \rangle_{[1,6]} = -0.15 \pm 0.16 \, . \tag{3.8}$$

However, with the current experimental accuracy, these observables are not sensitive enough to probe SUSY parameters.

---

[4]To be fully precise [45], we should multiply this number by a factor $(1 + y_s)/(1 + \mathcal{A}_{\Delta\Gamma} y_s)$ and compute the asymmetry $\mathcal{A}_{\Delta\Gamma}$ for the particular SUSY model studied. For most models passing this constraint, this factor is however less than a 2% correction.

4 Constraints on SUSY

To illustrate the impact of the recent limit on $\mathrm{BR}(B_s \to \mu^+\mu^-)$ and the measurements of the angular distributions and differential branching fraction of the $B \to K^*\mu^+\mu^-$ decay by LHCb, we consider constrained MSSM scenarios. The observables are calculated as described in section 2 using SuperIso v3.3 [34, 35].

We focus on two specific scenarios, both assuming SUSY breaking mediated by gravity and invoking unification boundary conditions at a very high scale m_{GUT} where the universal mass parameters are specified. The first model is the CMSSM, characterised by the set of parameters $\{m_0, m_{1/2}, A_0, \tan\beta, \mathrm{sgn}(\mu)\}$. Here m_0 is the universal mass of the scalars, $m_{1/2}$ the universal gaugino mass, A_0 the universal trilinear coupling, and $\tan\beta$ the ratio of the vacuum expectation values of the Higgs doublets. The second model we consider involves non-universal Higgs masses (NUHM). This model generalises the CMSSM, allowing for the GUT scale mass parameters of the Higgs doublets to have values different from m_0. The two additional parameters can be traded for two other parameters at a lower scale, conveniently the μ parameter and the mass M_A of the CP-odd Higgs boson implying that the charged Higgs boson mass can be treated essentially as a free parameter, contrary to the CMSSM. In both models, the flavour-changing effects we wish to study are effectively suppressed by the degeneracy of SUSY-breaking squark mass terms ($\sim m_0^2$ I) and trilinear couplings ($\sim A_0$ I) at the high scale, which suppresses the gluino (and neutralino) loop contributions. Only charged Higgs and chargino loops then remain, the latter dominating for large $\tan\beta > 30$. In this limit, the scalar penguin amplitudes get the strongest $\tan\beta$ enhancement. We thus expect the SUSY deviations from the SM to be maximised at large $\tan\beta$ for observables involving scalar penguin diagrams with a chargino-up-squark loop, for which the lightest stop mass should be a decisive parameter. Enlightening discussions of the large $\tan\beta$ limit and of the associated subtleties can be found in refs. [36–38].

First we study the constraints from $\mathrm{BR}(B_s \to \mu^+\mu^-)$ in the CMSSM. For this purpose, we scanned over $m_0 \in [100, 3000]\,\mathrm{GeV}$, $m_{1/2} \in [100, 3000]\,\mathrm{GeV}$, $A_0 \in [-5000, 2000]\,\mathrm{GeV}$ and $\tan\beta \in [1, 60]$, with $\mu > 0$. We generated about 500,000 points, and for each point we calculate the spectrum of SUSY particle masses and couplings using SOFTSUSY 3.2.4 [68] and compute $\mathrm{BR}(B_s \to \mu^+\mu^-)$ using SuperIso v3.3. The constraints are shown in figure 1 in the planes $(M_{\tilde{t}_1}, \tan\beta)$ and $(M_{H^\pm}, \tan\beta)$. These results could be compared to the previous results using the LHCb 2010 collected data [10, 69]. It is clear that the large values of $\tan\beta$ are strongly constrained.

In the NUHM scenario, the parameters are scanned over in a similar way as in the CMSSM, and in addition $\mu \in [-2000, 2000]\,\mathrm{GeV}$ and $M_A \in [50, 1100]\,\mathrm{GeV}$. The results are shown in figure 2. Since there are two additional degrees of freedom in NUHM as compared to CMSSM, it is easier for a model point to escape the constraint, as can be seen by comparing figures 1 and 2 where the allowed points are displayed on top. On the other hand since $M_{\tilde{t}_1}$ and $M_{H^\pm}$ are discorrelated in NUHM, it is possible for any $M_{\tilde{t}_1}$ to have a very small $M_{H^\pm}$ and therefore being excluded, as can be seen from the plot with the allowed points in the background.
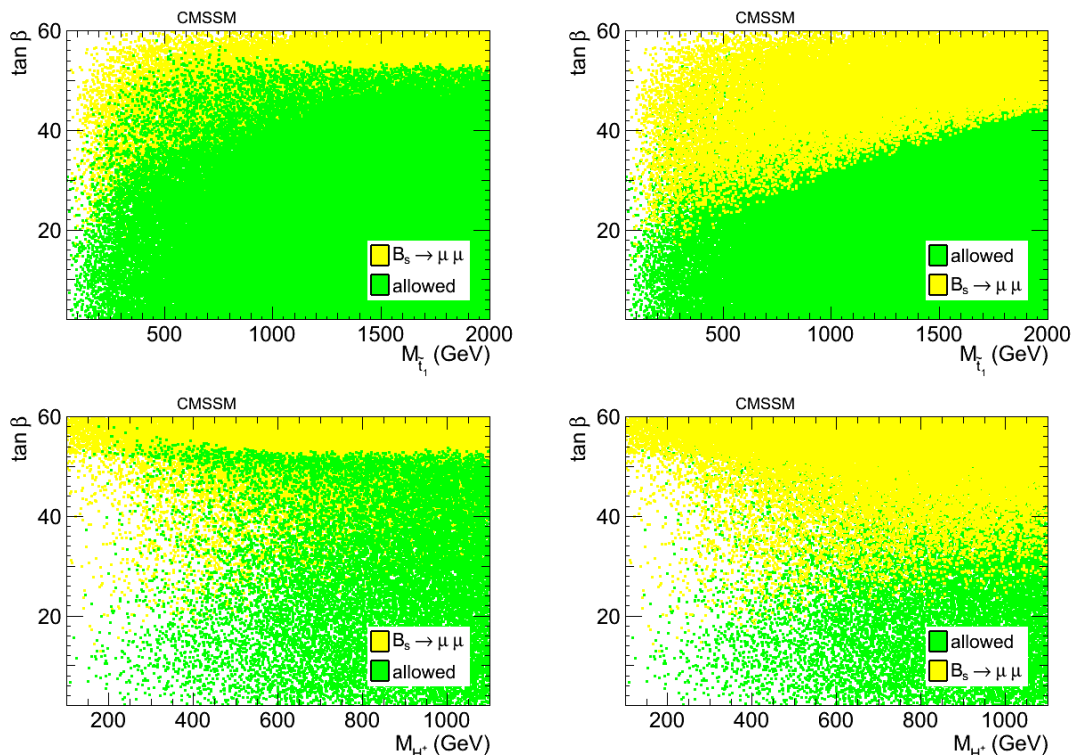
Figure 1. Constraint from $\mathrm{BR}(B_s \to \mu^+\mu^-)$ projected on the CMSSM planes $(M_{\tilde{t}_1}, \tan\beta)$ in the upper panel, and $(M_{H^\pm}, \tan\beta)$ in the lower panel. On the left, all green (dark grey) points satisfying the constraint are drawn last, hiding some excluded yellow (light grey) points; conversely on the right, all these excluded points are visible, hiding some allowed points.

The effect of an SM-like measurement of $\mathrm{BR}(B_s \to \mu^+\mu^-)$ in non-constrained MSSM (the pMSSM) is demonstrated in [70].

Next we consider the constraints from $B \to K^*\mu^+\mu^-$ observables. In order to study the maximal effects we consider $\tan\beta=50$ but show also the results for $\tan\beta=30$, and investigate the SUSY spread in function of the lightest stop mass. We start with the averaged differential branching ratio as defined in table 4. The results in CMSSM are displayed in figure 3 for the low q^2 region and in figure 4 for the high q^2 region, where the solid red lines correspond to the LHCb central value, while the dashed and dotted lines represent the 1 and 2σ bounds respectively, including both theoretical and experimental errors (added in quadrature). At low q^2, this branching ratio excludes $M_{\tilde{t}_1}$ below $\sim 250\,\mathrm{GeV}$ for $\tan\beta=50$ and $\sim 150\,\mathrm{GeV}$ for $\tan\beta=30$. In the high q^2 region the branching ratio is doing slightly better, as the $M_{\tilde{t}_1}$ below $\sim 300\,\mathrm{GeV}$ and $\sim 200\,\mathrm{GeV}$ are excluded for $\tan\beta=50$ and $\tan\beta=30$ respectively. As this light stop region is already excluded by the direct SUSY searches for the same scenario, $\mathrm{BR}(B \to K^*\mu^+\mu^-)$ does not provide additional information. The main reason of the limited constraining power of the branching ratio is the large theoretical uncertainties (mainly due to form factors) from which this observable is suffering. The results are shown for two values of A_0 ($=0$ and $-1000\,\mathrm{GeV}$) for comparison. As can be seen from the figures, the constraints with smaller A_0 are slightly stronger.

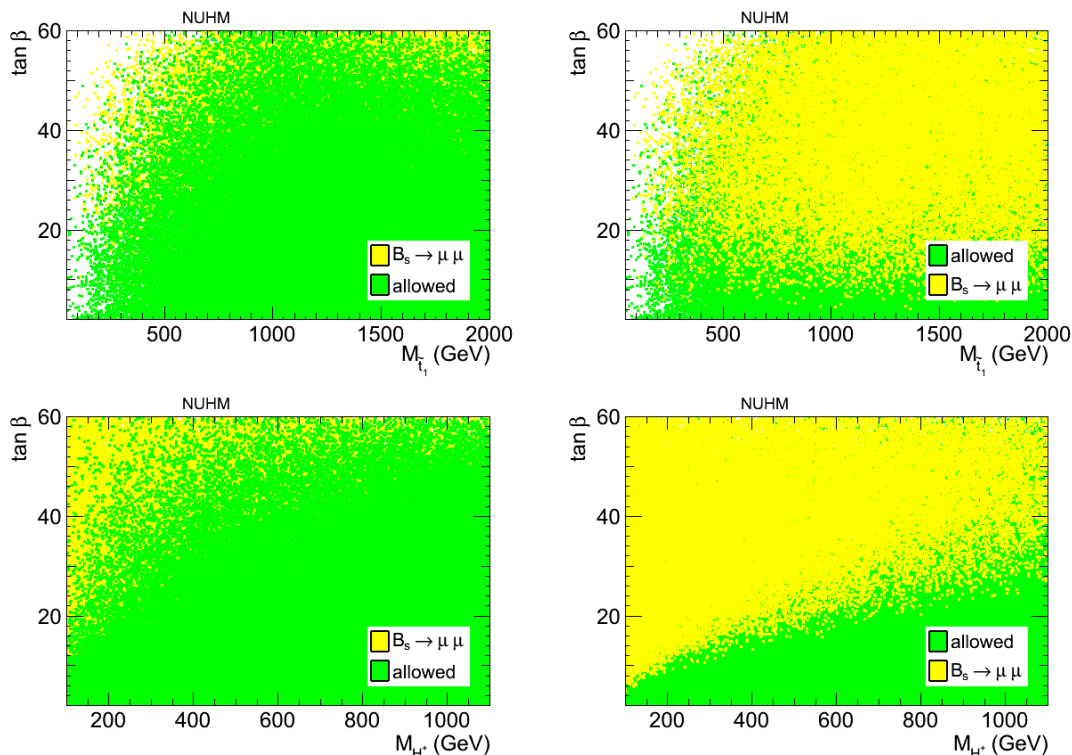**Figure 2**. Constraint from $BR(B_s \to \mu^+\mu^-)$ in the NUHM with the same conventions as in figure 1 for the CMSSM.

Contrary to the branching ratio, angular distributions, in which the theoretical uncertainties are reduced, can in principle provide more robust constraints on the SUSY parameter space. In particular, we consider in the following the forward-backward asymmetry A_{FB}, the zero-crossing q_0^2 of A_{FB}, F_L, as well as S_3, A_{Im} for which the LHCb results with $1\,\text{fb}^{-1}$ of data are available. The two latter observables do not provide any constraint with the current results and accuracy. The SUSY spread in function of the stop mass of A_{FB}, q_0^2 and F_L is given in figures 5–7. As can be seen, A_{FB} provides the most stringent constraints among these observables, and excludes $M_{\tilde{t}_1} \lesssim 800\,\text{GeV}$ and $600\,\text{GeV}$ at $\tan\beta=50$ and $\tan\beta=30$ respectively. q_0^2 on the other hand excludes $M_{\tilde{t}_1} \lesssim 550\,\text{GeV}$ (for $\tan\beta=50$) and $400\,\text{GeV}$ (for $\tan\beta=30$) while F_L excludes $M_{\tilde{t}_1} \lesssim 200\,\text{GeV}$ (for $\tan\beta=50$) and $150\,\text{GeV}$ (for $\tan\beta=30$). The impressive constraining power of A_{FB} is mainly due to the fact that the measured central value is smaller than the SM prediction and in addition the reported experimental errors are more than twice smaller than the previous results.

Same observables at high q^2 have less impact on the SUSY parameters and therefore their results are not reproduced here.

To illustrate the sensitivity of the observables to other SUSY parameters, in figure 8 we present the variation of A_{FB} (which has the largest impact as we have shown) with respect to the pseudo scalar Higgs mass and the gluino mass.

Another observable of interest for which LHCb has announced the measurement very recently [67] is the isospin asymmetry A_I, defined in eq. (2.18). Figure 9 illustrates the
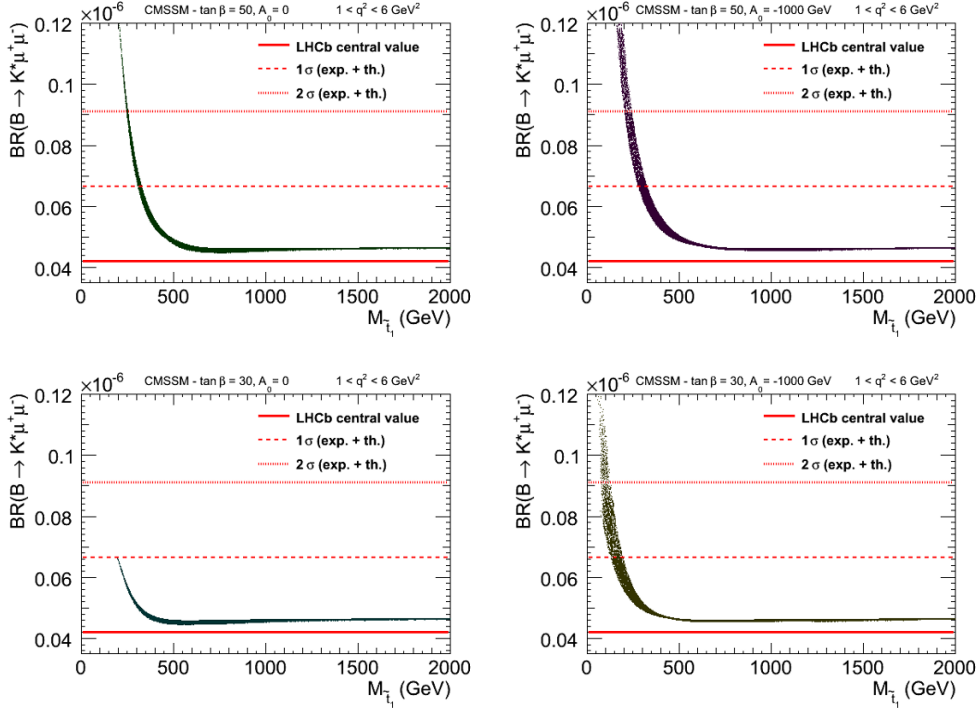
Figure 3. SUSY spread of the averaged BR$(B \to K^*\mu^+\mu^-)$ at low q^2 in function of the lightest stop mass, for $\tan\beta$=50 (upper panel) and $\tan\beta$=30 (lower panel), in the left for $A_0 = 0$ and in the right for $A_0 = -1000\,\mathrm{GeV}$.
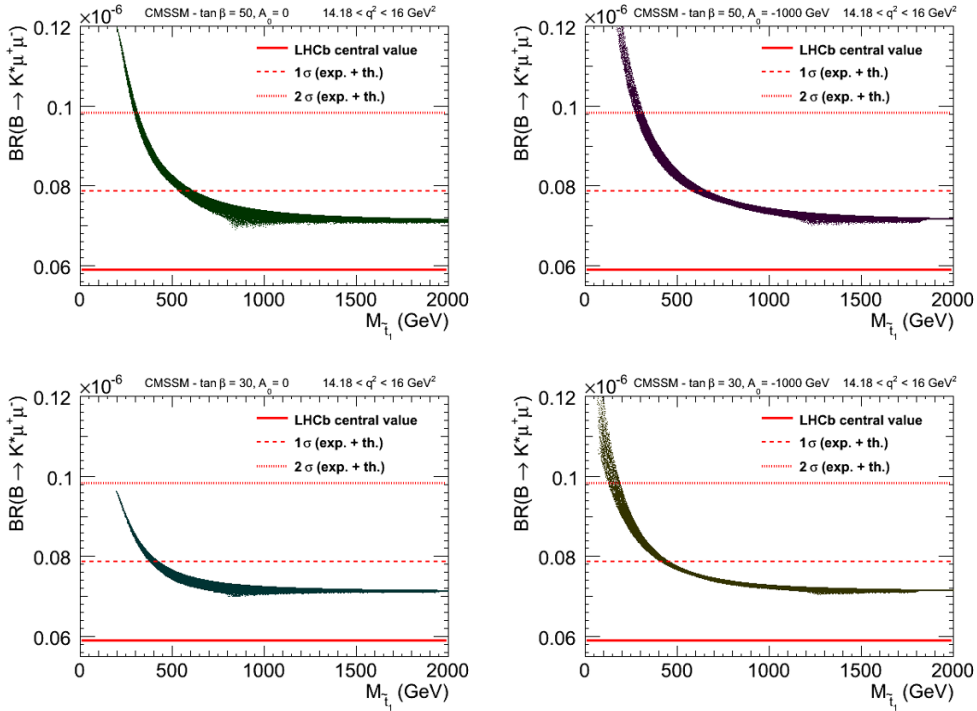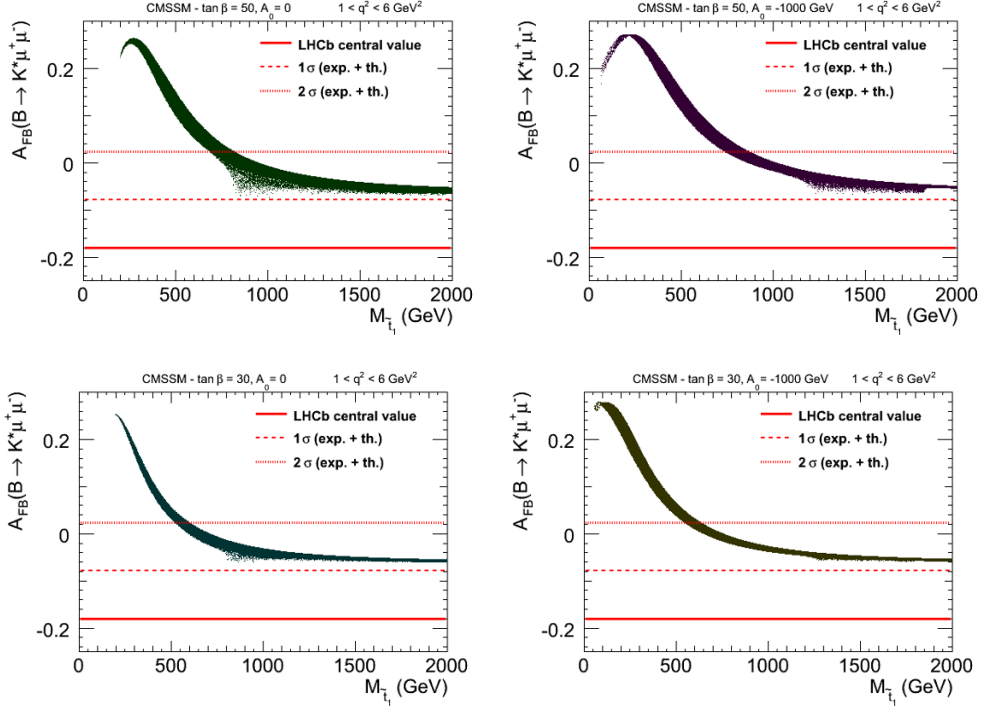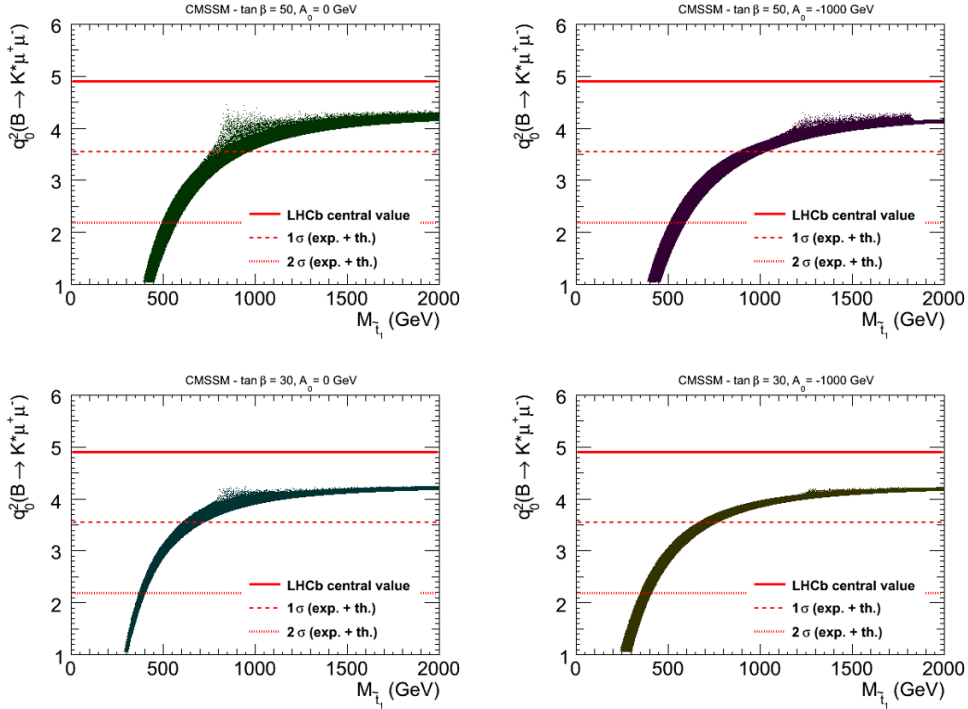

Figure 4. SUSY spread of the averaged BR$(B \to K^*\mu^+\mu^-)$ at high q^2, similar to figure 3.

Figure 5. SUSY spread of the $A_{FB}(B \to K^*\mu^+\mu^-)$ at low q^2 in function of the lightest stop mass, for $\tan\beta$=50 (upper panel) and $\tan\beta$=30 (lower panel), in the left for $A_0 = 0$ and in the right for $A_0 = -1000\,\text{GeV}$.

Figure 6. SUSY spread of the $A_{FB}(B \to K^*\mu^+\mu^-)$ zero-crossing, similar to figure 5.
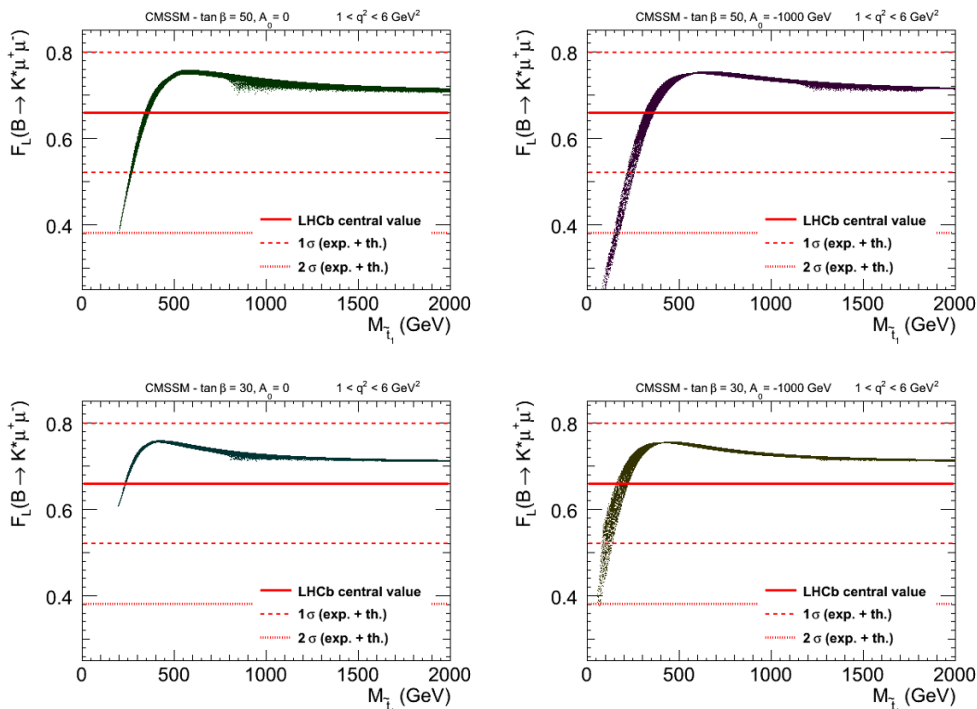
Figure 7. SUSY spread of the $F_L(B \to K^* \mu^+ \mu^-)$ at low q^2 in function of the lightest stop mass, for $\tan\beta$=50 (upper panel) and $\tan\beta$=30 (lower panel), in the left for $A_0 = 0$ and in the right for $A_0 = -1000\,\mathrm{GeV}$.
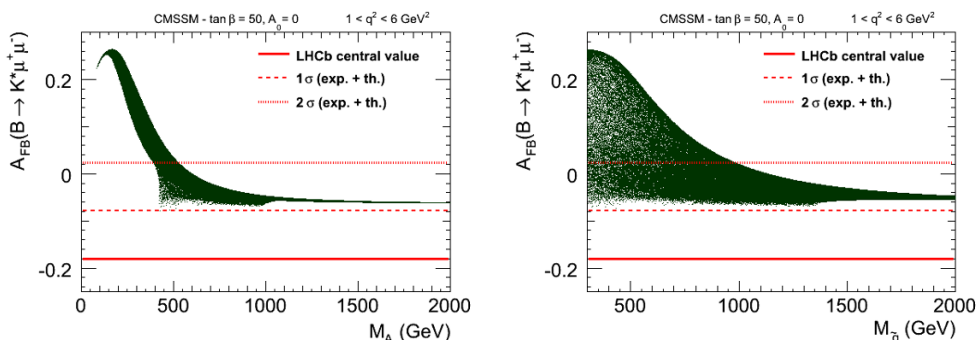

Figure 8. SUSY spread of the $A_{FB}(B \to K^* \mu^+ \mu^-)$ at low q^2 in function of the pseudo scalar Higgs mass (left) and the gluino mass (right), for $\tan\beta$=50 and $A_0 = 0$.

SUSY spread of A_I in function of $M_{\tilde{t}_1}$. Since the experimental measurement (eq. (3.8)) has an error larger than the SUSY spread, the current result does not provide any information on the SUSY parameters.

In figure 10, we show the SUSY spread in function of the lightest stop mass, for $A_T^{(2)}$, $A_T^{(3)}$, $A_T^{(4)}$ (defined in eqs. (2.19)–(2.21)) which are not measured yet by LHCb. Large deviations from the Standard Model can be seen for small values of $M_{\tilde{t}_1}$, and depending on their eventual upcoming experimental measurements they could be of interest in constraining SUSY parameters.
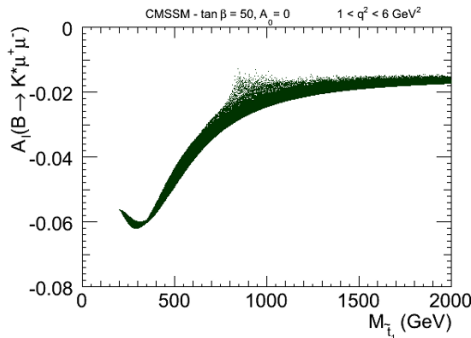
Figure 9. SUSY spread of the isospin asymmetry $(B \to K^* \mu^+ \mu^-)$ at low q^2 in function of the lightest stop mass, for $\tan \beta = 50$ and $A_0 = 0$.
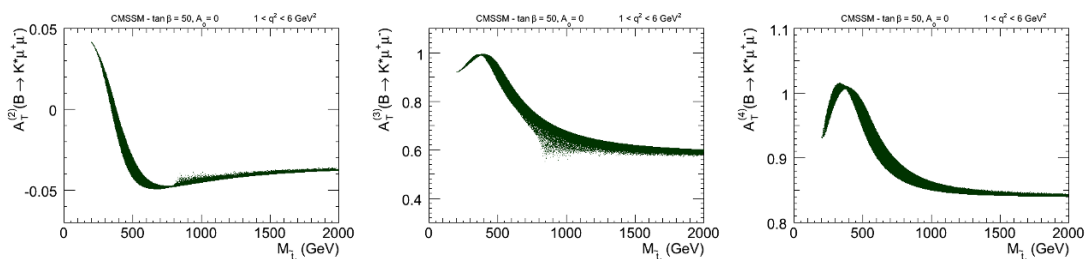

Figure 10. SUSY spread of $A_T^{(2)}$, $A_T^{(3)}$ and $A_T^{(4)}$ at low q^2 in function of the lightest stop mass, for $\tan \beta = 50$ and $A_0 = 0$.

A comparison between these observables in the plane $(m_{1/2}, m_0)$ is given in figure 11. As expected, A_{FB} is the most constraining observable also in this plane. All the observables show more sensitivity at larger $\tan \beta$ and more negative A_0. It should be noted that other indirect observables like $\mathrm{BR}(B \to X_s \gamma)$ briefly discussed below, or the branching ratio $A^0/H^0 \to \tau^+ \tau^-$ direct searches [71, 72] can independently bring comparable constraints [70].

To trace the origin of these constraints, it is interesting to present them in terms of Wilson coefficients. The variation of the observables in SUSY is driven on the one hand by the additional contributions to the Wilson Coefficients, in particular C_7, C_8, C_9 and C_{10}, and on the other hand by new contributions through the scalar and pseudo scalar coefficients C_{Q_1} and C_{Q_2}. The variation of the Wilson coefficients in a full CMSSM scan is presented in figure 12, ignoring existing constraints on SUSY parameters or Wilson coefficients. As can be seen, C_7 and C_8 can have both signs in SUSY and their correlation is visible in the figure: the same chargino-stop (or charged Higgs-top) loop gives the leading contribution, regardless of whether a photon (C_7) or gluon (C_8) is attached to it. As for C_9, it varies only by very little while C_{10} can have a larger spread. This feature can be understood once we notice that box diagrams are suppressed with respect to scalar- or Z-penguin diagrams, giving $\delta C_9/\delta C_{10} \sim (g_V/g_A)_\mu \sim 1 - 4 \sin^2 \theta_W$. On the other hand, scalar coefficients can receive very large contributions in SUSY, as already known. An interesting information can be obtained from the zero-crossing of A_{FB} since it depends on
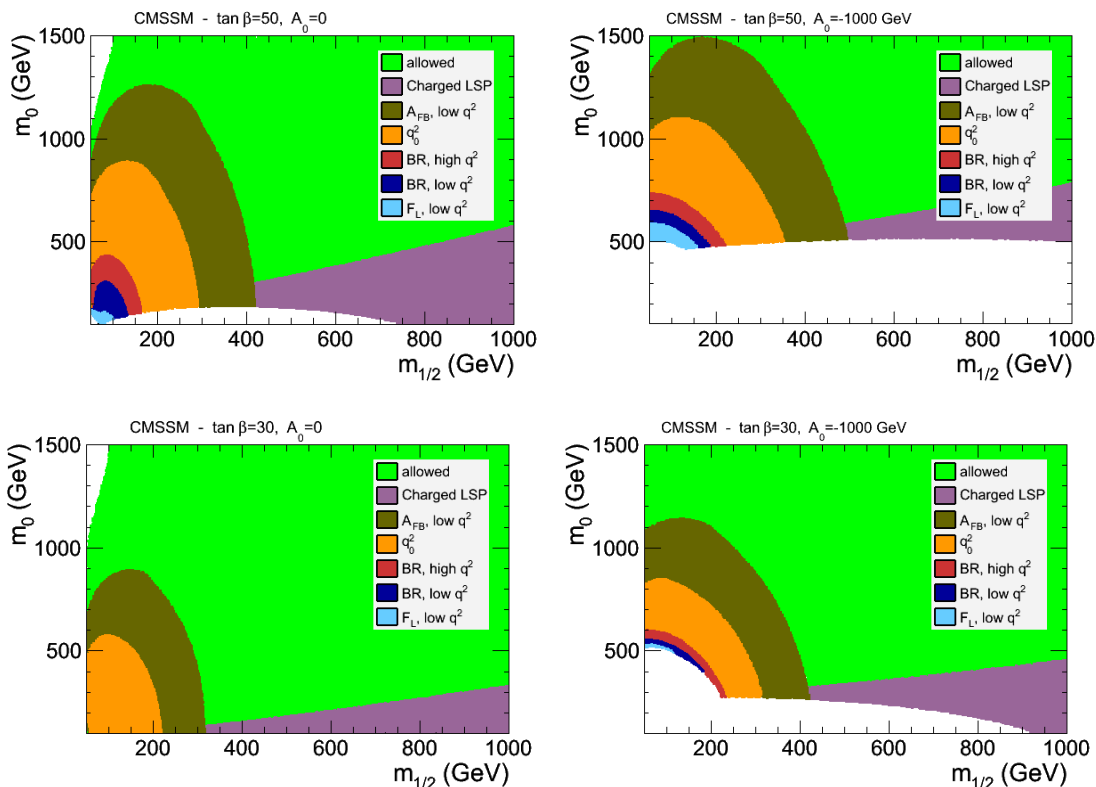
Figure 11. Constraining power of the $B \to K^* \mu^+ \mu^-$ observables in the plane $(m_{1/2}, m_0)$, for $\tan\beta$=50 (upper panel) and $\tan\beta$=30 (lower panel), in the left for $A_0 = 0$ and in the right for $A_0 = -1000 \, \text{GeV}$.

the relative sign of C_7 and C_9 as can be seen in eq. (2.17), and excludes the positive sign of C_7 as can be seen in figure 13.

Finally, in figure 14 we show the correlations of $\text{BR}(B \to X_s\gamma)$ with $\text{BR}(B \to K^*\mu^+\mu^-)$ and $A_{FB}(B \to K^*\mu^+\mu^-)$. In the SM, $\text{BR}(B \to X_s\gamma)$ is dominated by contributions from C_7. The SM prediction for this branching ratio is $(3.08 \pm 0.22) \times 10^{-4}$ [35, 73, 74] while the latest combined experimental value from HFAG is $(3.55 \pm 0.24 \pm 0.09) \times 10^{-4}$ [75]. As expected, there are strong correlations between $\text{BR}(B \to X_s\gamma)$ and $B \to K^*\mu^+\mu^-$ branching ratio and forward backward asymmetry, especially for small and intermediate values of $\tan\beta$, where the scalar and pseudo scalar contributions have a limited effect.

5   Conclusions

The rare decays $B_s \to \mu^+\mu^-$ and $B \to K^*\mu^+\mu^-$ are of great importance in exploring the footprints of physics beyond the SM. We have presented in this paper an update of the constraints by the recent LHCb limit on $\text{BR}(B_s \to \mu^+\mu^-)$ in two constrained MSSM scenarios, CMSSM and NUHM.

We also demonstrated that $B \to K^*\mu^+\mu^-$ provides a large number of complementary observables from the full angular distribution. In particular while $B_s \to \mu^+\mu^-$ lose very
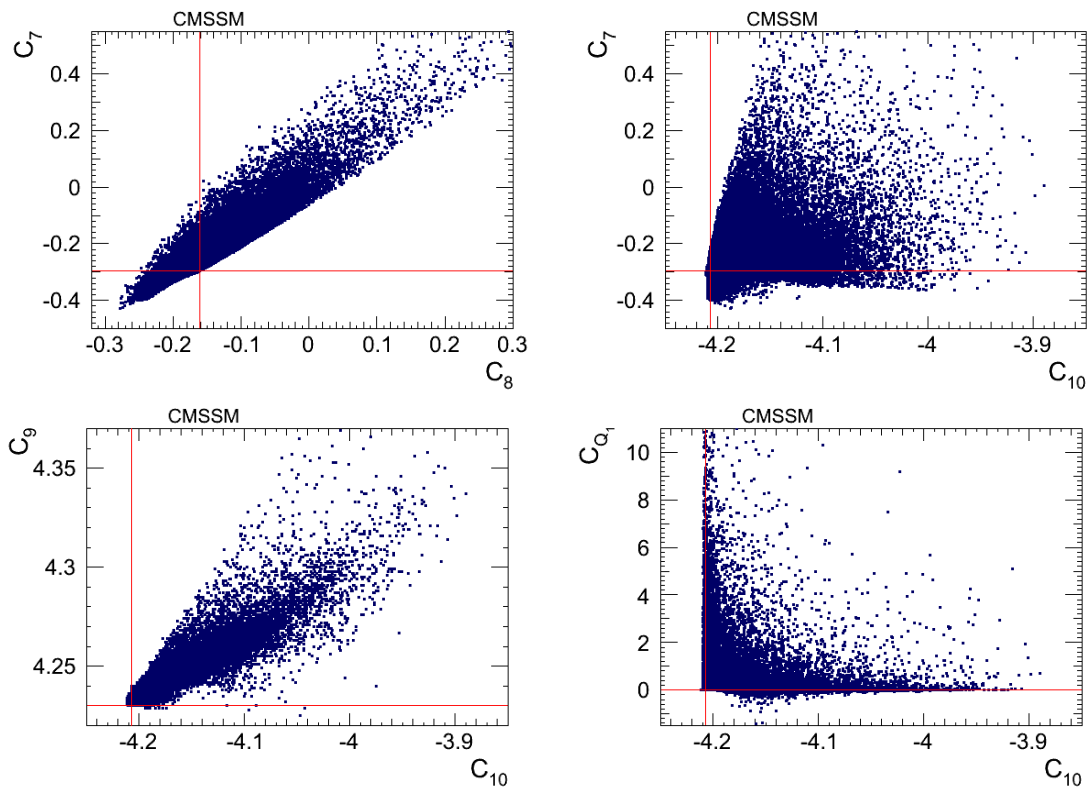
Figure 12. Variation of the Wilson coefficients in the CMSSM with all the parameters varied in the ranges given in the text. The red lines correspond to the SM predictions.
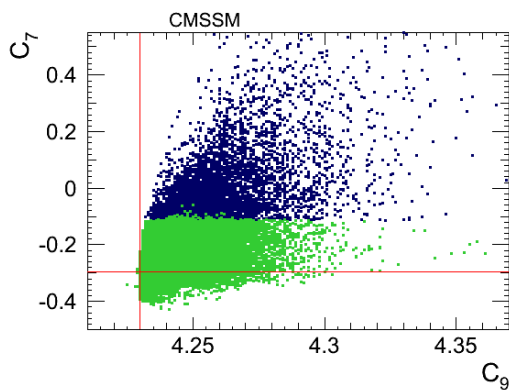

Figure 13. Variation of C_7 and C_9 in the CMSSM with all the parameters varied in the ranges given in the text. Only the green points are allowed by the zero-crossing of A_{FB}. The red lines correspond to the SM predictions.

rapidly its sensitivity by lowering down $\tan\beta$, the constraints by $B \to K^*\mu^+\mu^-$ observables weaken only mildly and thus act as additional tools to explore SUSY parameters. The forward backward asymmetry is in particular a very powerful observable which provides competitive information to the direct SUSY searches. To display the origin of these constraints in the CMSSM, we have shown the possible values and correlations between the
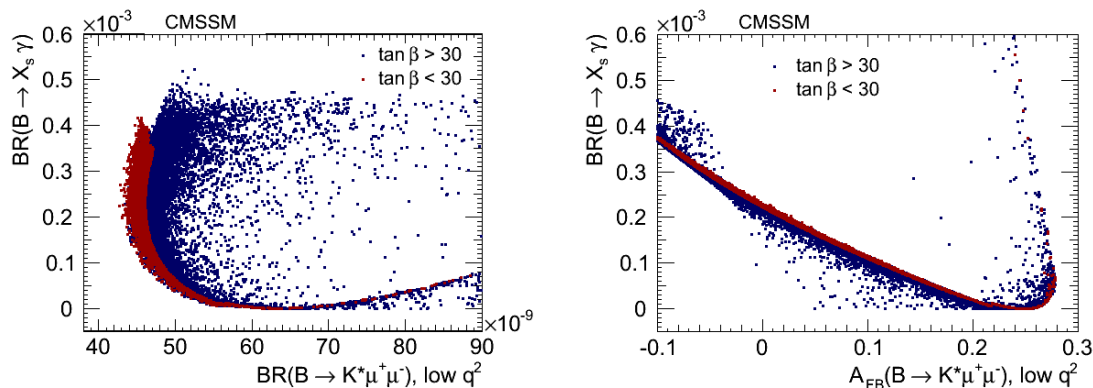
Figure 14. The correlation between $\mathrm{BR}(B \to X_s\gamma)$ and averaged $\mathrm{BR}(B \to K^*\mu^+\mu^-)$ in the left, and between $\mathrm{BR}(B \to X_s\gamma)$ and $A_{FB}(B \to K^*\mu^+\mu^-)$ in the right.

Wilson coefficients of the various operators relevant for these processes. Among those, the Wilson coefficient C_9 is a parameter for which these angular observables provide a unique handle. However, we have shown that the sensitivity of C_9 to CMSSM effects is suppressed by the muon vector coupling, because they proceed mainly through a Z penguin diagram. The constraining power of other observables, like the isospin asymmetry whose measurement is under way, have been shown to display their interest in the framework of Minimal Flavour Violation models for which the CMSSM provides an interesting prototype.

With reduced theoretical and experimental errors for these observables, in particular for the forward backward asymmetry and its zero-crossing which have been recently measured for the first time by the LHCb experiment, one would have access to very powerful observables in constraining supersymmetric models. The information obtained in this way can also serve as consistency checks with the results of the direct searches.

A Angular coefficients J_i

The angular coefficients are given below [22].

$$J_1^s = \frac{(2 + \beta_\ell^2)}{4} \left[|A_\perp^L|^2 + |A_\parallel^L|^2 + (L \to R)\right] + \frac{4m_\ell^2}{q^2}\mathrm{Re}\left(A_\perp^L A_\perp^{R*} + A_\parallel^L A_\parallel^{R*}\right) , \tag{A.1a}$$

$$J_1^c = |A_0^L|^2 + |A_0^R|^2 + \frac{4m_\ell^2}{q^2}\left[|A_t|^2 + 2\mathrm{Re}(A_0^L A_0^{R*})\right] + \beta_\ell^2|A_S|^2 , \tag{A.1b}$$

$$J_2^s = \frac{\beta_\ell^2}{4}\left[|A_\perp^L|^2 + |A_\parallel^L|^2 + (L \to R)\right] , \tag{A.1c}$$

$$J_2^c = -\beta_\ell^2\left[|A_0^L|^2 + (L \to R)\right] , \tag{A.1d}$$

$$J_3 = \frac{1}{2}\beta_\ell^2\left[|A_\perp^L|^2 - |A_\parallel^L|^2 + (L \to R)\right] , \tag{A.1e}$$

$$J_4 = \frac{1}{\sqrt{2}}\beta_\ell^2\left[\mathrm{Re}(A_0^L A_\parallel^{L*}) + (L \to R)\right] , \tag{A.1f}$$

– 20 –

$$J_5 = \sqrt{2}\beta_\ell \left[\text{Re}(A_0^L A_\perp^{L\,*}) - (L \to R) - \frac{m_\ell}{\sqrt{q^2}} \text{Re}(A_\parallel^L A_S^* + A_\parallel^R A_S^*) \right] , \tag{A.1g}$$

$$J_6^s = 2\beta_\ell \left[\text{Re}(A_\parallel^L A_\perp^{L\,*}) - (L \to R) \right] , \tag{A.1h}$$

$$J_6^c = 4\beta_\ell \frac{m_\ell}{\sqrt{q^2}} \text{Re} \left[A_0^L A_S^* + (L \to R) \right] , \tag{A.1i}$$

$$J_7 = \sqrt{2}\beta_\ell \left[\text{Im}(A_0^L A_\parallel^{L\,*}) - (L \to R) + \frac{m_\ell}{\sqrt{q^2}} \text{Im}(A_\perp^L A_S^* + A_\perp^R A_S^*) \right] , \tag{A.1j}$$

$$J_8 = \frac{1}{\sqrt{2}}\beta_\ell^2 \left[\text{Im}(A_0^L A_\perp^{L\,*}) + (L \to R) \right] , \tag{A.1k}$$

$$J_9 = \beta_\ell^2 \left[\text{Im}(A_\parallel^{L\,*} A_\perp^L) + (L \to R) \right] . \tag{A.1l}$$

with β_ℓ defined in eq. (2.10).

B Form factors

The $\mathcal{T}_{\perp,\parallel}$ (which include non-factorisable corrections) are described in terms of the soft form factors and can be found in [13, 14] where, in order to get $\mathcal{T}_{\perp,\parallel}^\pm$, C_7^{eff} appearing in $\mathcal{T}_{\perp,\parallel}$ should be replaced with $(C_7^{\text{eff}} \pm C_7')$ [23]. To obtain the soft form factors we have used the factorisation scheme used in [14]:

$$\xi_\perp(q^2) = \frac{M_B}{M_B + m_{K^*}} V(q^2) , \tag{B.1}$$

$$\xi_\parallel(q^2) = \frac{M_B + m_{K^*}}{2E_{K^*}} A_1(q^2) - \frac{M_B - m_{K^*}}{M_B} A_2(q^2) . \tag{B.2}$$

The full form factors V and $A_{1,2}$ have been taken from light-cone sum rule (LCSR) calculations [58]:

$$V(q^2) = \frac{r_1}{1 - q^2/m_R^2} + \frac{r_2}{1 - q^2/m_{fit}^2} , \tag{B.3}$$

$$A_1(q^2) = \frac{r_2}{1 - q^2/m_{fit}^2} , \tag{B.4}$$

$$A_2(q^2) = \frac{r_1}{1 - q^2/m_{fit}^2} + \frac{r_2}{(1 - q^2/m_{fit}^2)^2} , \tag{B.5}$$

where the fit parameters $r_{1,2}, m_R^2$ and m_{fit}^2 are given in table 6.

C Renormalisation group equations for C_9

To obtain the evolved Wilson coefficients from the matching scale (μ_0) to μ_b, the renormalisation group equation (RGE) for $\vec{\tilde{C}}$ has to be solved:

$$\mu \frac{d}{d\mu} \vec{\tilde{C}}(\mu) = \hat{\gamma}^T(g) \vec{\tilde{C}}(\mu) , \tag{C.1}$$

	r_1	r_2	$m_R^2\,[\text{GeV}^2]$	$m_{fit}^2\,[\text{GeV}^2]$
V	0.923	-0.511	5.32^2	49.40
A_1		0.290		40.38
A_2	-0.084	0.342		52.00

Table 6. Fit parameters describing the q^2 dependence of the form factors V and $A_{1,2}$ in the LCSR approach [58].

where $\hat{\gamma}$ is the Anomalous Dimension Matrix (ADM). A general solution for the RGE is

$$\vec{\tilde{C}}(\mu_b) = \hat{U}(\mu_b, \mu_0)\vec{\tilde{C}}(\mu_0)\,, \tag{C.2}$$

where $\hat{U}$ is the evolution matrix

$$\hat{U}(\mu_b, \mu_0) = T_g \exp \int_{g(\mu_0)}^{g(\mu_b)} dg' \frac{(\hat{\gamma}^T(g'))}{\beta(g')}\,. \tag{C.3}$$

T_g is the $g(=\sqrt{4\pi\alpha_s})$-ordering operator such that the coupling constants increase from right to left. $\hat{\gamma}$ and β can be expanded in g

$$\hat{\gamma}(g) = \frac{g^2}{16\pi^2}\hat{\gamma}^{(0)} + \left(\frac{g^2}{16\pi^2}\right)^2 \hat{\gamma}^{(1)} + \left(\frac{g^2}{16\pi^2}\right)^3 \hat{\gamma}^{(2)} + \dots \tag{C.4}$$

$$\beta(g) = -\frac{g^3}{16\pi^2}\beta_0 - \frac{g^5}{(16\pi^2)^2}\beta_1 - \frac{g^7}{(16\pi^2)^4}\beta_2 + \dots \tag{C.5}$$

The Wilson coefficients and the evolution matrix expanded in α_s are

$$\hat{U}(\mu_b, \mu_0) = \sum_{n \geqslant 0} \left(\frac{\alpha_s(\mu_0)}{4\pi}\right)^{(n)} \hat{U}^{(n)} \tag{C.6}$$

$$\vec{\tilde{C}}_i(\mu) = \sum_{n \geqslant 0} \left(\frac{\alpha_s(\mu)}{4\pi}\right)^{(n)} \vec{\tilde{C}}_i^{(n)}(\mu). \tag{C.7}$$

Following the conventions used in [41], the evolution matrix is

$$U_{kl}^{(n)} = \sum_{j=0}^{n} \sum_{i=1}^{9} m_{kli}^{(nj)} \eta^{a_i - j} \tag{C.8}$$

where $\eta = \alpha_s(\mu_0)/\alpha_s(\mu_b)$.

Using the above relations for the different orders of $C_9(\mu_b)$ we have

$$\tilde{C}_9^{(0)}(\mu_b) = \sum_{l=1}^{9} U_{9l}^{(0)} \tilde{C}_l^{(0)}(\mu_0) \tag{C.9}$$

$$\tilde{C}_9^{(1)}(\mu_b) = \eta \left[\sum_{l=1}^{9} U_{9l}^{(0)} \tilde{C}_l^{(1)}(\mu_0) + \sum_{l=1}^{9} U_{9l}^{(1)} \tilde{C}_l^{(0)}(\mu_0) \right] \tag{C.10}$$

$$\tilde{C}_9^{(2)}(\mu_b) = \eta^2 \left[\sum_{l=1}^{9} U_{9l}^{(0)} \tilde{C}_l^{(2)}(\mu_0) + \sum_{l=1}^{9} U_{9l}^{(1)} \tilde{C}_l^{(1)}(\mu_0) + \sum_{l=1}^{9} U_{9l}^{(2)} \tilde{C}_l^{(0)}(\mu_0) \right]. \tag{C.11}$$

i	1	2	3	4	5	6	7	8	9
a_i	$\frac{14}{23}$	$\frac{16}{23}$	$\frac{6}{23}$	$-\frac{12}{23}$	0.4086	-0.4230	-0.8994	0.1456	-1

Table 7. The numbers a_i used in eq. (C.8).

i	1	2	3	4	5	6	7	8	9
$m_{91i}^{(00)}$	0	0	-0.0328	-0.0404	0.0021	-0.0289	-0.0174	-0.0010	0.1183
$m_{92i}^{(00)}$	0	0	-0.0985	0.0606	0.0108	0.0346	0.0412	-0.0018	-0.0469
$m_{93i}^{(00)}$	0	0	0	0	0.0476	-0.1167	-0.3320	-0.0718	0.4729
$m_{94i}^{(00)}$	0	0	0	0	0.0318	0.0918	-0.2700	0.0059	0.1405
$m_{95i}^{(00)}$	0	0	0	0	0.9223	-2.4126	-1.5972	-0.4870	3.57455
$m_{96i}^{(00)}$	0	0	0	0	0.4245	1.1742	-0.0507	-0.0293	-1.5186
$m_{99i}^{(00)}$	0	0	0	0	0	0	0	0	1

Table 8. "Magic numbers" $m_{9li}^{(00)}$.

To obtain the evolution matrix we have followed [76] and [77]. Taking $\hat{\gamma}^{(0)}$, $\hat{\gamma}^{(1)}$ and $\hat{\gamma}^{(2)}$ from [41] and [78], we have produced the necessary "magic numbers" (m_{kli}) for the evaluation of U_{9l}. Since O_9 does not mix with $O_{7,8}$ the magic numbers m_{97i} and m_{98i} are all zero. The a_i's and the rest of the m_{kli} can be found in tables 7–13.

In the above formulas, $\tilde{C}_l^{(n)}(\mu_0)$ for $l \neq 7, 8$ can all be found in section 2 of [79] where to get our $\tilde{C}_l^{(n)}(\mu_0)$ we use $\tilde{C}_l^{(n)}(\mu_0) = C_l^{t(n)}(\mu_0) - C_l^{c(n)}(\mu_0)$, and $\tilde{C}_{7,8}^{(n)}(\mu_0)$ are not needed since U_{97} and U_{98} are zero. To get the Wilson coefficients based on our choice of operators (eq. (2.2)) we have

$$C_9(\mu_b) = \frac{4\pi}{\alpha_s(\mu_b)} \tilde{C}_9. \tag{C.12}$$

Acknowledgments

i	1	2	3	4	5	6	7	8	9
$m_{91i}^{(10)}$	0	0	0.1958	-0.0442	-0.0112	-0.1111	0.1283	0.0114	-0.3596
$m_{92i}^{(10)}$	0	0	0.2917	0.2482	0.0382	0.1331	-0.2751	0.0260	-0.8794
$m_{93i}^{(10)}$	0	0	0	0	-0.1041	-0.5696	9.5004	0.0396	-0.4856
$m_{94i}^{(10)}$	0	0	0	0	-0.0126	-0.4049	-0.6870	0.1382	0.4172
$m_{95i}^{(10)}$	0	0	0	0	4.7639	-35.0057	30.7862	5.5105	62.3651
$m_{96i}^{(10)}$	0	0	0	0	-1.9027	-1.8789	-43.9516	1.9612	54.4557
$m_{99i}^{(10)}$	0	0	0	0	0	0	0	0	0

Table 9. "Magic numbers" $m_{9li}^{(10)}$.

i	1	2	3	4	5	6	7	8	9
$m_{91i}^{(11)}$	0	0	0.2918	0.0484	-0.0331	-0.0269	0.0200	-0.1094	0
$m_{92i}^{(11)}$	0	0	0.8754	-0.0725	-0.1685	0.0323	-0.0475	-0.2018	0
$m_{93i}^{(11)}$	0	0	0	0	-0.7405	-0.1088	0.3825	-7.9139	0
$m_{94i}^{(11)}$	0	0	0	0	-0.4942	0.0856	0.3111	0.6465	0
$m_{95i}^{(11)}$	0	0	0	0	-14.3464	-2.2495	1.8402	-53.6643	0
$m_{96i}^{(11)}$	0	0	0	0	-6.6029	1.0948	0.0584	-3.2339	0
$m_{99i}^{(11)}$	0	0	0	0	0	0	0	0	0

Table 10. "Magic numbers" $m_{9li}^{(11)}$.

i	1	2	3	4	5	6	7	8	9
$m_{91i}^{(20)}$	0	0	0.6878	-0.9481	-0.1928	-0.8077	-0.2554	0.0562	-0.6436
$m_{92i}^{(20)}$	0	0	1.3210	3.1616	-0.4814	1.9362	-5.0873	0.0468	-13.5825
$m_{93i}^{(20)}$	0	0	0	0	-2.5758	-5.8751	0.0922	0.6433	7.7756
$m_{94i}^{(20)}$	0	0	0	0	-2.6194	1.1302	-27.7073	-0.8550	16.0333
$m_{95i}^{(20)}$	0	0	0	0	-6.4519	-555.931	35.1531	80.2925	102.043
$m_{96i}^{(20)}$	0	0	0	0	-53.3822	34.3969	-124.609	-32.7515	-98.8845
$m_{99i}^{(20)}$	0	0	0	0	0	0	0	0	0

Table 11. "Magic numbers" $m_{9li}^{(20)}$.

i	1	2	3	4	5	6	7	8	9
$m_{91i}^{(21)}$	0	0	-1.7394	0.0530	0.1741	-0.1036	-0.1478	1.2522	0
$m_{92i}^{(21)}$	0	0	-2.5918	-0.2971	-0.5949	0.1241	0.3170	2.8655	0
$m_{93i}^{(21)}$	0	0	0	0	1.6188	-0.5311	-10.9454	4.36311	0
$m_{94i}^{(21)}$	0	0	0	0	0.1967	-0.3775	0.7915	15.2328	0
$m_{95i}^{(21)}$	0	0	0	0	-74.1049	-32.6399	-35.4688	607.188	0
$m_{96i}^{(21)}$	0	0	0	0	29.5971	-1.7519	50.6366	216.094	0
$m_{99i}^{(21)}$	0	0	0	0	0	0	0	0	0

Table 12. "Magic numbers" $m_{9li}^{(21)}$.

i	1	2	3	4	5	6	7	8	9
$m_{91i}^{(22)}$	0	0	4.1531	-0.4627	-0.3404	-1.0326	0.0809	0.2167	0
$m_{92i}^{(22)}$	0	0	12.4592	0.6940	-1.7340	1.2360	-0.1921	0.3998	0
$m_{93i}^{(22)}$	0	0	0	0	-7.6198	-4.1683	1.5484	15.674	0
$m_{94i}^{(22)}$	0	0	0	0	-5.0848	3.2810	1.2592	-1.2804	0
$m_{95i}^{(22)}$	0	0	0	0	-147.615	-86.199	7.4486	106.285	0
$m_{96i}^{(22)}$	0	0	0	0	-67.9394	41.9523	0.2364	6.405	0
$m_{99i}^{(22)}$	0	0	0	0	0	0	0	0	0

Table 13. "Magic numbers" $m_{9li}^{(22)}$.

References

[1] S.R. Choudhury and N. Gaur, *Dileptonic decay of B_s meson in SUSY models with large* $\tan\beta$, *Phys. Lett.* **B 451** (1999) 86 [hep-ph/9810307] [INSPIRE].

[2] K. Babu and C.F. Kolda, *Higgs mediated $B^0 \to \mu^+\mu^-$ in minimal supersymmetry*, *Phys. Rev. Lett.* **84** (2000) 228 [hep-ph/9909476] [INSPIRE].

[3] C.-S. Huang, W. Liao, Q.-S. Yan and S.-H. Zhu, *$B_s \to lepton + lepton$ — In a general 2HDM and MSSM*, *Phys. Rev.* **D 63** (2001) 114021 [*Erratum ibid.* **D 64** (2001) 059902] [hep-ph/0006250] [INSPIRE].

[4] J.R. Ellis, K.A. Olive and V.C. Spanos, *On the interpretation of $B_s \to \mu^+\mu^-$ in the CMSSM*, *Phys. Lett.* **B 624** (2005) 47 [hep-ph/0504196] [INSPIRE].

[5] M.S. Carena, A. Menon, R. Noriega-Papaqui, A. Szynkman and C. Wagner, *Constraints on B and Higgs physics in minimal low energy supersymmetric models*, *Phys. Rev.* **D 74** (2006) 015009 [hep-ph/0603106] [INSPIRE].

[6] J.R. Ellis, S. Heinemeyer, K. Olive and G. Weiglein, *Light heavy MSSM Higgs bosons at large* tan β, *Phys. Lett.* **B 653** (2007) 292 [arXiv:0706.0977] [ɪɴSPIRE].

[7] F. Mahmoudi, *New constraints on supersymmetric models from* $b \to s\gamma$, *JHEP* **12** (2007) 026 [arXiv:0710.3791] [ɪɴSPIRE].

[8] D. Eriksson, F. Mahmoudi and O. Stal, *Charged Higgs bosons in minimal supersymmetry: updated constraints and experimental prospects*, *JHEP* **11** (2008) 035 [arXiv:0808.3551] [ɪɴSPIRE].

[9] E. Golowich, J. Hewett, S. Pakvasa, A.A. Petrov and G.K. Yeghiyan, *Relating* B_s *mixing and* $B_s \to \mu^+\mu^-$ *with new physics*, *Phys. Rev.* **D 83** (2011) 114017 [arXiv:1102.0009] [ɪɴSPIRE].

[10] A. Akeroyd, F. Mahmoudi and D.M. Santos, *The decay* $B_s \to \mu^+\mu^-$: *updated SUSY constraints and prospects*, *JHEP* **12** (2011) 088 [arXiv:1108.3018] [ɪɴSPIRE].

[11] LHCʙ collaboration, R. Aaij et al., *Strong constraints on the rare decays* $B_s \to \mu^+\mu^-$ *and* $B^0 \to \mu^+\mu^-$, *Phys. Rev. Lett.* **108** (2012) 231801 [arXiv:1203.4493] [ɪɴSPIRE].

[12] CDF collaboration, T. Aaltonen et al., *Search for* $B_s \to \mu^+\mu^-$ *and* $B_d \to \mu^+\mu^-$ *Decays with CDF II*, *Phys. Rev. Lett.* **107** (2011) 239903 [arXiv:1107.2304] [ɪɴSPIRE].

[13] M. Beneke, T. Feldmann and D. Seidel, *Systematic approach to exclusive* $B \to V\ell^+\ell^-$, $V\gamma$ *decays*, *Nucl. Phys.* **B 612** (2001) 25 [hep-ph/0106067] [ɪɴSPIRE].

[14] M. Beneke, T. Feldmann and D. Seidel, *Exclusive radiative and electroweak* $b \to d$ *and* $b \to s$ *penguin decays at NLO*, *Eur. Phys. J.* **C 41** (2005) 173 [hep-ph/0412400] [ɪɴSPIRE].

[15] F. Krüger and J. Matias, *Probing new physics via the transverse amplitudes of* $B^0 \to K^{*0}(\to K^-\pi^+)\ell^+\ell^-$ *at large recoil*, *Phys. Rev.* **D 71** (2005) 094009 [hep-ph/0502060] [ɪɴSPIRE].

[16] U. Egede, T. Hurth, J. Matias, M. Ramon and W. Reece, *New observables in the decay mode* $\bar{B}_d) \to \bar{K}^{*0}\ell^+\ell^-$, *JHEP* **11** (2008) 032 [arXiv:0807.2589] [ɪɴSPIRE].

[17] A. Ali, P. Ball, L. Handoko and G. Hiller, *A comparative study of the decays* $B \to (K, K^*)\ell^+\ell^-$ *in standard model and supersymmetric theories*, *Phys. Rev.* **D 61** (2000) 074024 [hep-ph/9910221] [ɪɴSPIRE].

[18] G. Buchalla, G. Hiller and G. Isidori, *Phenomenology of nonstandard Z couplings in exclusive semileptonic* $b \to s$ *transitions*, *Phys. Rev.* **D 63** (2000) 014015 [hep-ph/0006136] [ɪɴSPIRE].

[19] F. Krüger and E. Lunghi, *Looking for novel CP-violating effects in* $\bar{B} \to K^*\ell^+\ell^-$, *Phys. Rev.* **D 63** (2001) 014013 [hep-ph/0008210] [ɪɴSPIRE].

[20] T. Feldmann and J. Matias, *Forward backward and isospin asymmetry for* $B \to K^*\ell^+\ell^-$ *decay in the standard model and in supersymmetry*, *JHEP* **01** (2003) 074 [hep-ph/0212158] [ɪɴSPIRE].

[21] E. Lunghi and J. Matias, *Huge right-handed current effects in* $B \to K^*(K\pi)\ell^+\ell^-$ *in supersymmetry*, *JHEP* **04** (2007) 058 [hep-ph/0612166] [ɪɴSPIRE].

[22] W. Altmannshofer et al., *Symmetries and asymmetries of* $B \to K^*\mu^+\mu^-$ *decays in the standard model and beyond*, *JHEP* **01** (2009) 019 [arXiv:0811.1214] [ɪɴSPIRE].

[23] C. Bobeth, G. Hiller and G. Piranishvili, *CP asymmetries in bar* $B \to \bar{K}^*(\to \bar{K}\pi)\ell\ell$ *and untagged* $\bar{B}_s$, $B_s \to \phi(\to K^+K^-)\ell\ell$ *decays at NLO*, *JHEP* **07** (2008) 106 [arXiv:0805.2525] [ɪɴSPIRE].

[24] U. Egede, T. Hurth, J. Matias, M. Ramon and W. Reece, *New physics reach of CP-violating observables in the decay* $\bar{B}_d \to \bar{K}^*\ell^+\ell^-$, PoS(EPS-HEP2009)184 [arXiv:0912.1349] [ɪɴSPIRE].

[25] U. Egede, T. Hurth, J. Matias, M. Ramon and W. Reece, *New physics reach of the decay mode $\bar{B} \to \bar{K}^{*0}\ell^+\ell^-$*, *JHEP* **10** (2010) 056 [arXiv:1005.0571] [INSPIRE].

[26] C. Bobeth, G. Hiller and D. van Dyk, *The benefits of $\bar{B} \to \bar{K}^* l^+ l^-$ decays at low recoil*, *JHEP* **07** (2010) 098 [arXiv:1006.5013] [INSPIRE].

[27] E. Lunghi and A. Soni, *An improved observable for the forward-backward asymmetry in $B \to K^*\ell^+\ell^-$ and $B_s \to \phi\ell^+\ell^-$*, *JHEP* **11** (2010) 121 [arXiv:1007.4015] [INSPIRE].

[28] A.K. Alok et al., *New physics in $b \to s\mu^+\mu^-$: CP-conserving observables*, *JHEP* **11** (2011) 121 [arXiv:1008.2367] [INSPIRE].

[29] A.K. Alok et al., *New physics in $b \to s\mu^+\mu^-$: CP-violating observables*, *JHEP* **11** (2011) 122 [arXiv:1103.5344] [INSPIRE].

[30] C. Bobeth, G. Hiller and D. van Dyk, *More benefits of semileptonic rare B decays at low recoil: CP-violation*, *JHEP* **07** (2011) 067 [arXiv:1105.0376] [INSPIRE].

[31] A. Behring, C. Gross, G. Hiller and S. Schacht, *Squark flavor implications from $B \to K^*\ell^+\ell^-$*, arXiv:1205.1500 [INSPIRE].

[32] F. Mahmoudi, *Direct and indirect searches for new physics*, arXiv:1205.3099 [INSPIRE].

[33] LHCB collaboration, *Differential branching fraction and angular analysis of the $B^0 \to K^{*0}\mu^+\mu^-$ decay*, LHCb-CONF-2012-008 (2012).

[34] F. Mahmoudi, *SuperIso: a program for calculating the isospin asymmetry of $B \to K^*\gamma$ in the MSSM*, *Comput. Phys. Commun.* **178** (2008) 745 [arXiv:0710.2067] [INSPIRE].

[35] F. Mahmoudi, *SuperIso v2.3: a program for calculating flavor physics observables in supersymmetry*, *Comput. Phys. Commun.* **180** (2009) 1579 [arXiv:0808.3144] [INSPIRE].

[36] G. Isidori and A. Retico, *Scalar flavor changing neutral currents in the large $\tan\beta$ limit*, *JHEP* **11** (2001) 001 [hep-ph/0110121] [INSPIRE].

[37] A.J. Buras, P.H. Chankowski, J. Rosiek and L. Slawianowska, *$\Delta M_{d,s}$, $B_{d,s}^0 \to \mu^+\mu^-$ and $B \to X_s\gamma$ in supersymmetry at large $\tan\beta$*, *Nucl. Phys.* **B 659** (2003) 3 [hep-ph/0210145] [INSPIRE].

[38] C. Bobeth, T. Ewerth, F. Krüger and J. Urban, *Enhancement of $B(\bar{B}_d) \to \mu^+\mu^- / B(\bar{B}_s) \to \mu^+\mu^-$ in the MSSM with minimal flavor violation and large $\tan\beta$*, *Phys. Rev.* **D 66** (2002) 074021 [hep-ph/0204225] [INSPIRE].

[39] K.G. Chetyrkin, M. Misiak and M. Münz, *$|\Delta F| = 1$ nonleptonic effective Hamiltonian in a simpler scheme*, *Nucl. Phys.* **B 520** (1998) 279 [hep-ph/9711280] [INSPIRE].

[40] Q.-S. Yan, C.-S. Huang, W. Liao and S.-H. Zhu, *Exclusive semileptonic rare decays $B \to (K, K^*)\ell^+\ell^-$ in supersymmetric theories*, *Phys. Rev.* **D 62** (2000) 094023 [hep-ph/0004262] [INSPIRE].

[41] M. Czakon, U. Haisch and M. Misiak, *Four-loop anomalous dimensions for radiative flavour-changing decays*, *JHEP* **03** (2007) 008 [hep-ph/0612329] [INSPIRE].

[42] LHCB collaboration, *Tagged time-dependent angular analysis of $B_s^0 \to J/\psi\phi$ decays at LHCb*, LHCb-CONF-2012-002 (2012).

[43] S. Descotes-Genon, J. Matias and J. Virto, *An analysis of $B_{d,s}$ mixing angles in presence of new physics and an update of $B_s \to K^{0*}\bar{K}^{0*}$*, *Phys. Rev.* **D 85** (2012) 034010 [arXiv:1111.4882] [INSPIRE].

[44] K. de Bruyn et al., *Branching ratio measurements of B_s decays*, *Phys. Rev.* **D 86** (2012) 014027 [arXiv:1204.1735] [INSPIRE].

[45] K. de Bruyn et al., *Probing new physics via the $B_s^0 \to \mu^+\mu^-$ effective lifetime*, *Phys. Rev. Lett.* **109** (2012) 041801 [arXiv:1204.1737] [INSPIRE].

[46] C. Bobeth, T. Ewerth, F. Krüger and J. Urban, *Analysis of neutral Higgs boson contributions to the decays $\bar{B}_s \to \ell^+\ell^-$ and $\bar{B} \to K\ell^+\ell^-$*, *Phys. Rev.* **D 64** (2001) 074014 [hep-ph/0104284] [INSPIRE].

[47] ETM collaboration, P. Dimopoulos et al., *Lattice QCD determination of m_b, f_B and f_{B_s} with twisted mass Wilson fermions*, *JHEP* **01** (2012) 046 [arXiv:1107.1441] [INSPIRE].

[48] FERMILAB LATTICE AND MILC COLLABORATIONS collaboration, A. Bazavov et al., *B- and D-meson decay constants from three-flavor lattice QCD*, *Phys. Rev.* **D 85** (2012) 114506 [arXiv:1112.3051] [INSPIRE].

[49] FERMILAB LATTICE AND MILC collaboration, E. Neil et al., *B and D meson decay constants from $2 + 1$ flavor improved staggered simulations*, PoS(LATTICE 2011)320 [arXiv:1112.3978] [INSPIRE].

[50] H. Na et al., *The B and B_s meson decay constants from lattice QCD*, arXiv:1202.4914 [INSPIRE].

[51] C. McNeile, C. Davies, E. Follana, K. Hornbostel and G. Lepage, *High-precision f_{B_s} and HQET from relativistic lattice QCD*, *Phys. Rev.* **D 85** (2012) 031503 [arXiv:1110.4510] [INSPIRE].

[52] C. Davies, *Standard model heavy flavor physics on the lattice*, PoS(LATTICE 2011)019 [arXiv:1203.3862] [INSPIRE].

[53] J. Laiho et al., *$2 + 1$ flavor lattice QCD averages*, http://www.latticeaverages.org/.

[54] C. Bobeth, P. Gambino, M. Gorbahn and U. Haisch, *Complete NNLO QCD analysis of $\bar{B} \to X_s\ell^+\ell^-$ and higher order electroweak effects*, *JHEP* **04** (2004) 071 [hep-ph/0312090] [INSPIRE].

[55] J. Charles et al., *Predictions of selected flavour observables within the standard model*, *Phys. Rev.* **D 84** (2011) 033005 [arXiv:1106.4041] [INSPIRE].

[56] PARTICLE DATA GROUP collaboration, K. Nakamura et al., *Review of particle physics*, *J. Phys.* **G 37** (2010) 075021, and 2011 partial update for the 2012 edition [INSPIRE].

[57] P. Ball, V. Braun and A. Lenz, *Twist-4 distribution amplitudes of the K^* and ϕ mesons in QCD*, *JHEP* **08** (2007) 090 [arXiv:0707.1201] [INSPIRE].

[58] P. Ball and R. Zwicky, *$B_{d,s} \to \rho, \omega, K^*, \phi$ decay form-factors from light-cone sum rules revisited*, *Phys. Rev.* **D 71** (2005) 014029 [hep-ph/0412079] [INSPIRE].

[59] P. Ball and R. Zwicky, *$|V_{td}/V_{ts}|$ from $B \to V\gamma$*, *JHEP* **04** (2006) 046 [hep-ph/0603232] [INSPIRE].

[60] J. Charles, A. Le Yaouanc, L. Oliver, O. Pene and J. Raynal, *Heavy to light form-factors in the heavy mass to large energy limit of QCD*, *Phys. Rev.* **D 60** (1999) 014001 [hep-ph/9812358] [INSPIRE].

[61] M. Beneke and T. Feldmann, *Symmetry breaking corrections to heavy to light B meson form-factors at large recoil*, *Nucl. Phys.* **B 592** (2001) 3 [hep-ph/0008255] [INSPIRE].

[62] F. Krüger, L.M. Sehgal, N. Sinha and R. Sinha, *Angular distribution and CP asymmetries in the decays $\bar{B} \to K^-\pi^+e^-e^+$ and $\bar{B} \to \pi^-\pi^+e^-e^+$*, *Phys. Rev.* **D 61** (2000) 114028 [*Erratum ibid.* **D 63** (2001) 019901] [hep-ph/9907386] [INSPIRE].

[63] J. Matias, F. Mescia, M. Ramon and J. Virto, *Complete anatomy of $\bar{B}_d -> \bar{K}^{*0}(\to K\pi)\ell^+\ell^-$ and its angular distribution*, *JHEP* **04** (2012) 104 [arXiv:1202.4266] [INSPIRE].

[64] B. Grinstein and D. Pirjol, *Exclusive rare $B \to K^* \ell^+ \ell^-$ decays at low recoil: controlling the long-distance effects*, *Phys. Rev.* **D 70** (2004) 114005 [hep-ph/0404250] [INSPIRE].

[65] C. Bobeth, G. Hiller, D. van Dyk and C. Wacker, *The decay $B \to K \ell^+ \ell^-$ at low hadronic recoil and model-independent $\Delta B = 1$ constraints*, *JHEP* **01** (2012) 107 [arXiv:1111.2558] [INSPIRE].

[66] CMS collaboration, S. Chatrchyan et al., *Search for $B_s^0 \to \mu^+ \mu^-$ and $B^0 \to \mu^+ \mu^-$ decays*, *JHEP* **04** (2012) 033 [arXiv:1203.3976] [INSPIRE].

[67] LHCb collaboration, R. Aaij et al., *Measurement of the isospin asymmetry in $B \to K^{(*)} \mu^+ \mu^-$ decays*, *JHEP* **07** (2012) 133 [arXiv:1205.3422] [INSPIRE].

[68] B. Allanach, *SOFTSUSY: a program for calculating supersymmetric spectra*, *Comput. Phys. Commun.* **143** (2002) 305 [hep-ph/0104145] [INSPIRE].

[69] LHCb collaboration, R. Aaij et al., *Search for the rare decays $B_s \to \mu^+ \mu^-$ and $B^0 \to \mu^+ \mu^-$*, *Phys. Lett.* **B 708** (2012) 55 [arXiv:1112.1600] [INSPIRE].

[70] A. Arbey, M. Battaglia and F. Mahmoudi, *Constraints on the MSSM from the Higgs sector: a pMSSM study of Higgs searches, $B_s^0 \to \mu^+ \mu^-$ and dark matter direct detection*, *Eur. Phys. J.* **C 72** (2012) 1906 [arXiv:1112.3032] [INSPIRE].

[71] CMS collaboration, S. Chatrchyan et al., *Search for neutral Higgs bosons decaying to tau pairs in pp collisions at $\sqrt{s} = 7$ TeV*, *Phys. Lett.* **B 713** (2012) 68 [arXiv:1202.4083] [INSPIRE].

[72] ATLAS collaboration, G. Aad et al., *Search for the standard model Higgs boson in the $H \to \tau^+ \tau^-$ decay mode in $\sqrt{s} = 7$ TeV pp collisions with ATLAS*, arXiv:1206.5971 [INSPIRE].

[73] M. Misiak and M. Steinhauser, *NNLO QCD corrections to the $\bar{B} \to X_s \gamma$ matrix elements using interpolation in m_c*, *Nucl. Phys.* **B 764** (2007) 62 [hep-ph/0609241] [INSPIRE].

[74] M. Misiak et al., *Estimate of $B(\bar{B} \to X_s \gamma)$ at $O(\alpha_s^2)$*, *Phys. Rev. Lett.* **98** (2007) 022002 [hep-ph/0609232] [INSPIRE].

[75] HEAVY FLAVOR AVERAGING GROUP collaboration, D. Asner et al., *Averages of b-hadron, c-hadron and τ-lepton Properties*, arXiv:1010.1589 [INSPIRE].

[76] A.J. Buras, *Climbing NLO and NNLO summits of weak decays*, arXiv:1102.5650 [INSPIRE].

[77] A.J. Buras, M. Gorbahn, U. Haisch and U. Nierste, *Charm quark contribution to $K^+ \to \pi^+ \nu \bar{\nu}$ at next-to-next-to-leading order*, *JHEP* **11** (2006) 002 [hep-ph/0603079] [INSPIRE].

[78] P. Gambino, M. Gorbahn and U. Haisch, *Anomalous dimension matrix for radiative and rare semileptonic B decays up to three loops*, *Nucl. Phys.* **B 673** (2003) 238 [hep-ph/0306079] [INSPIRE].

[79] C. Bobeth, M. Misiak and J. Urban, *Photonic penguins at two loops and m_t dependence of $BR(B \to X_s \ell^+ \ell^-)$*, *Nucl. Phys.* **B 574** (2000) 291 [hep-ph/9910220] [INSPIRE].